Deutsches Zentrum
für Luft- und Raumfahrt e.V.

Final Report IB554-06/02

Cooling System for a Ka Band Transmit Antenna Array

Björn J. Döring

Institute of Communications and Navigation
Oberpfaffenhofen

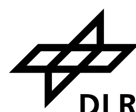

Deutsches Zentrum
für Luft- und Raumfahrt e.V.
in der Helmholtz-Gemeinschaft

Cooling System for a Ka Band
Transmit Antenna Array

Björn J. Döring

Institute of Communications and
Navigation
Oberpfaffenhofen

70 Seiten
28 Bilder
5 Tabellen
57 Literaturstellen

Cooling System for a Ka Band Transmit Antenna Array

Deutsches Zentrum
für Luft- und Raumfahrt e.V.

This work was submitted as a diploma thesis at the Technical University Berlin on
December 19, 2005.

Abstract

Active antenna arrays working at higher frequencies result in higher packaging densities. The antenna array under consideration operates at about 30 GHz and will be installed in an aircraft. Commercially available power amplifiers at these frequencies have an efficiency of typically 20 %, which results in high amounts of dissipated heat for the required high radiated power. The dissipated power, up to 9.5 kW as a worst case for a 50×50 element array, has to be transfered from the antenna to a heat exchanger or to the ambient air. Several cooling techniques including forced air and liquid cooling as well as heat pipes will be presented in this work, always considering the packaging density and the little space available. Simulations based on the software Flotherm led to the result that a liquid cooled cold plate is the most feasible approach while meeting all requirements. Experiments on a simplified model and comparison with simulations confirmed the results. Additionally, a forced air convection fin heat sink based on standard components was proposed, which can be used for an antenna demonstration model with 4×4 elements.

Zusammenfassung

Aktive Antennenarrays, die bei höheren Frequenzen betrieben werden, ziehen eine höhere Bauteildichte nach sich. Das zu untersuchende Array arbeitet bei rund 30 GHz und wird in Flugzeugen installiert werden. Kommerziell verfügbare Leistungsverstärker aber haben in diesem Frequenzbereich nur einen Wirkungsgrad von typischerweise 20 %. Dies bewirkt eine hohe Verlustleistung nicht zuletzt aufgrund der hohen benötigten Sendeleistung. Die Verlustleistung, die im ungünstigsten Fall 9,5 kW für ein Array mit 50 $\times$ 50 Elementen betragen kann, muss vom Inneren der Antenne zu einem Wärmetauscher oder an die Umgebungsluft abgeführt werden. Mehrere Kühlmethoden inklusive der erzwungenen Luft- und Wasserkühlung sowie die Kühlung mit Wärmerohren werden im Rahmen dieser Arbeit vorgestellt, wobei die hohe Bauteildichte und der geringe zur Verfügung stehende Platz berücksichtigt wird. Simulationen, die mit der Software Flotherm durchgeführt wurden, ergaben, dass ein wassergekühltes System die am besten praktikable Lösung unter Beachtung der Randbedingungen ist. Messungen an einem verkleinerten Modell und der Abgleich mit Simulationsergebnissen haben dies bestätigt. Zusätzlich wurde ein aus Standardelementen aufgebautes Lüfter-Kühlsystem untersucht, das für ein Demonstrations-Array mit 4 $\times$ 4 Elementen genutzt werden kann.

Contents

1 Symbols **1**

2 Introduction **3**

3 Project constraints **5**
3.1 Assembly constraints 5
3.2 Environmental conditions 7
3.2.1 Temperature 7
3.2.2 Air pressure and density 8
3.2.3 Humidity 9
3.2.4 Mechanical conditions 9
3.3 Amplifier 9
3.4 Heat spreader and heat sink materials 11

4 Heat transfer theory **15**
4.1 Heat conduction 15
4.2 Convection 17
4.2.1 Dynamical similarity and dimensionless numbers. 17
4.2.2 Natural convection 19
4.2.3 Forced convection 19
4.3 Thermal radiation 22

5 Software **23**
5.1 Thermal Desktop 23
5.2 Flotherm 24

6 Cooling techniques **25**
6.1 Natural convection air cooling 25
6.2 Forced air cooling 26
6.2.1 Influence of altitude 29
6.2.2 Possible designs and simulations 33
6.3 Forced liquid cooling – Cold plates 38
6.3.1 Design considerations 40

6.3.2 Design for 50 × 50 elements 41
6.3.3 Coolants 42
6.3.4 Simulation 43
6.3.5 Perspective 44
6.4 Peltier coolers 44
6.5 Heat pipes 44
6.5.1 Micro heat pipes 46
6.5.2 Conlusion 46
6.6 Other cooling techniques 47

7 Experiments 49
7.1 Design 49
7.2 Thermometer 50
7.3 Experimental setup and execution 51
7.4 Simulation 52
7.5 Sources of error 54
7.6 Results and discussion 55
7.7 Improvements 56

8 Heat exchanger 57

9 Conclusion 59

A Detailed drawings and pictures of cold plate 61

Bibliography 67

1 Symbols

Symbol	Name	SI unit
A	Surface	m^2
G	Volumetric flow rate	$m^3\,s^{-1}$
L	Length	m
Nu	Nusselt number	1
P	Power	W
Pr	Prandtl number	1
$\dot{Q}$	Heat flux	W
R	Gas constant for specific gas	$J\,K^{-1}\,kg^{-1}$
R_{th}	Thermal resistance	$K\,W^{-1}$
Ra	Rayleigh number	1
Re	Reynolds number	1
T	Temperature	K
U	Wetted perimeter	m
a	Thermal diffusivity	$m^2\,s^{-1}$
c	Specific heat	$J\,kg^{-1}\,K^{-1}$
d	Diameter	m
h	Heat transfer coefficient	$W\,m^{-1}\,K^{-1}$
l	Length	m
$\dot{m}$	Mass flow rate	$kg\;\;s^{-1}$
p	Pressure	Pa
$\dot{q}$	Heat flux density	$W\,m^{-2}$
v	Fluid velocity	$m\,s^{-1}$
x_e	Entrance region	m
δ	Fluid flow boundary layer thickness	m
δ_T	Temperature layer thickness	m
η	Dynamic viscosity	$kg\,m^{-1}\,s^{-1}$
λ	Thermal conductivity	$W\,m^{-1}\,K^{-1}$
ν	Kinematic viscosity	$m^2\,s^{-1}$
ρ	Density	$kg\,m^{-3}$
ω	Angular speed	$rad\,s^{-1}$

2 Introduction

This diploma thesis is aimed at developing a cooling system for an active Ka band transmit antenna array.

There is an increasing demand for in-flight aircraft broadband multimedia and communication services. In order to provide global coverage, satellite based solutions are necessary. Although commercial systems are already available, several drawbacks exist. Major disadvantages are the limited bandwidth of the utilized L and Ku band channels and *mechanical* beam steering. The ATENAA project, as explained below, focuses on the higher frequency Ka band (20/30 GHz) with a mechanically fixed (and therefore maintenance free and fast steering) flat active antenna array to overcome both disadvantages.

Microwave power amplifiers are necessary to reach the required radiated power levels. Typical efficiencies are as low as 20 %, which result in high dissipated power levels. This combined with high packing densities due to the small wavelengths and an avionics environment poses special challenges for a cooling system.

The central and not previously answered question was if cooling of the antenna array is generally possible despite the high packing density. Several cooling techniques were considered, and it showed that a liquid cooled system is the most promising approach. In the course of the project, development was based on numerical simulations. The simulations for a liquid cooled system were experimentally verified on a simplified model.

This work is part of the Advanced Technologies for Networking in Avionic Applications (ATENAA) project.[1] ATENAA is part of the sixth framework program of the European Union. Its main research interests are mobile ad-hoc networks, in- and outside optical communication links, and Ka band communication systems. The antenna group of the German Aerospace Center (Deutsches Zentrum für Luft- und Raumfahrt – DLR) focuses on the development of a test bed for mobile broadband satellite communications for both transmission and reception.

Due to the investigative nature of the ATENAA project, the focus of development was the cooling of the antenna array and not the complete cooling system. This means that the integration of the system into the aircraft structure and an additional heat exchanger (which is necessary for a coolant loop) are beyond the scope of this document. Nevertheless, basic ideas on heat exchangers for a liquid cooled system are presented in Chapter 8.

[1] http://www.atenna.org

3 Project constraints

3.1 Assembly constraints

The transmit antenna array operates at about 30 GHz. The radiating elements, patches, are positioned on a flat surface each one half of a free-space wavelength or 5 mm [1] as can be seen in Fig. 3.1. The elements are arranged in a square. The more patches, the better is the antenna performance in terms of directivity. Although different numbers of elements are possible, an array with 50×50 elements (and therefore a base plate dimension of 25×25 cm^2) seems to be the most likely choice at this stage of the ATENAA project. An array with up to 100×100 elements is possible as well.

Due to the small wavelength and a resulting high packaging density, integration of all required parts including the cooling system is a major problem. Figure 3.2 outlines the principle layer structure of the antenna array. The topmost layer (neglecting a possible radom) is the substrate with the radiating patch. It is connected by vias or by means of aperture coupling to a layer featuring a network and the power amplifiers. The power amplifiers are directly mounted on a yet to be specified cold plate. The power amplifiers are connected to the feeding network using connectors. Therefore, the cold plate has to incorporate cut outs which will feature the connectors. Although their final dimensions might still change during the course of the project, they are assumed to be 3 mm wide and 10 mm long. Furthermore, the connectors are assumed to be able to bridge a cold-plate thickness of maximal 5 mm. Two connectors will be necessary for a sub-assembly of 4×4 radiating elements as shown in Fig. 3.3. The cut outs diminish the available surface area, and therefore the amplifiers have to be placed closer to each other. Furthermore, the cut outs limit the available locations for fluid channels through the cold plate.

No cooling system elements can be placed in the direction in which the antenna radiates since the antenna pattern would be significantly influenced. The same is true for the bottom side since all space is taken up by electronics as indicated in Figs. 3.1 and 3.2. Therefore, heat has to be transfered to the sides of the array where it can finally be dissipated. This and a maximal cold plate thickness of 5 mm are the main factors which govern the final cold plate design.

An apparent disadvantage of these constraints is that no heat can be extracted from several spots in the middle of the array. This increases the temperature difference across the array which can produce phase errors. This is due to the amplifiers whose operating points are affected by temperature. Temperature differences across the array can nevertheless be compensated to some degree by calibration of the array.

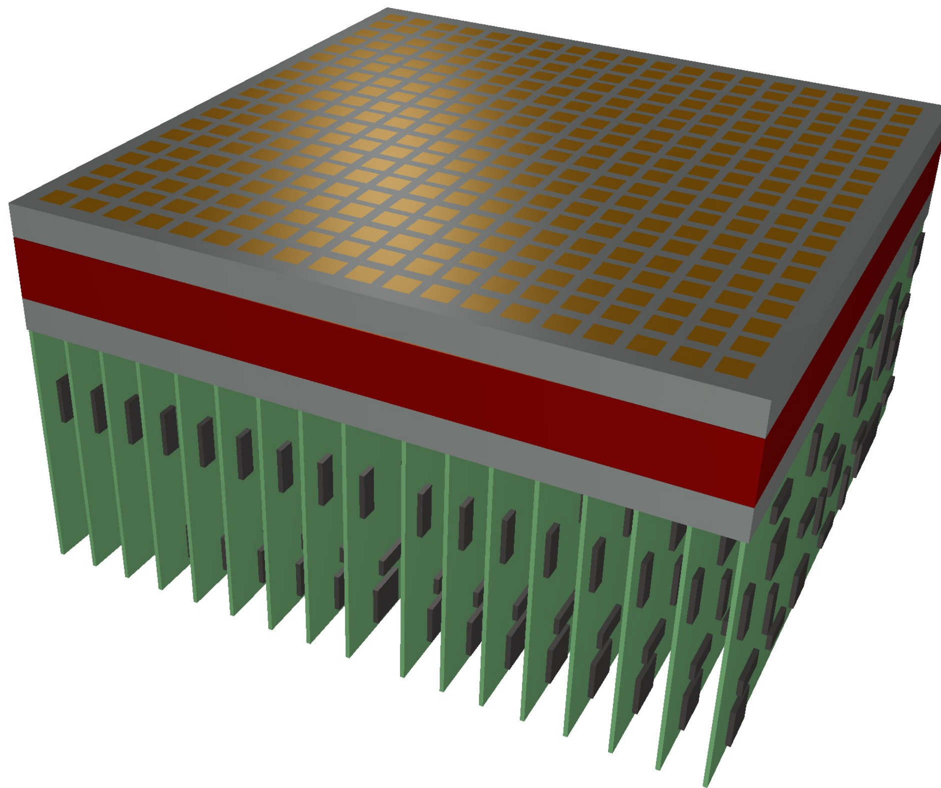

Figure 3.1: Sketch of the complete antenna array. The red layer indicates the position of the cold plate. The design and location of circuit boards is not decided yet; they are just shown for illustrational reasons.

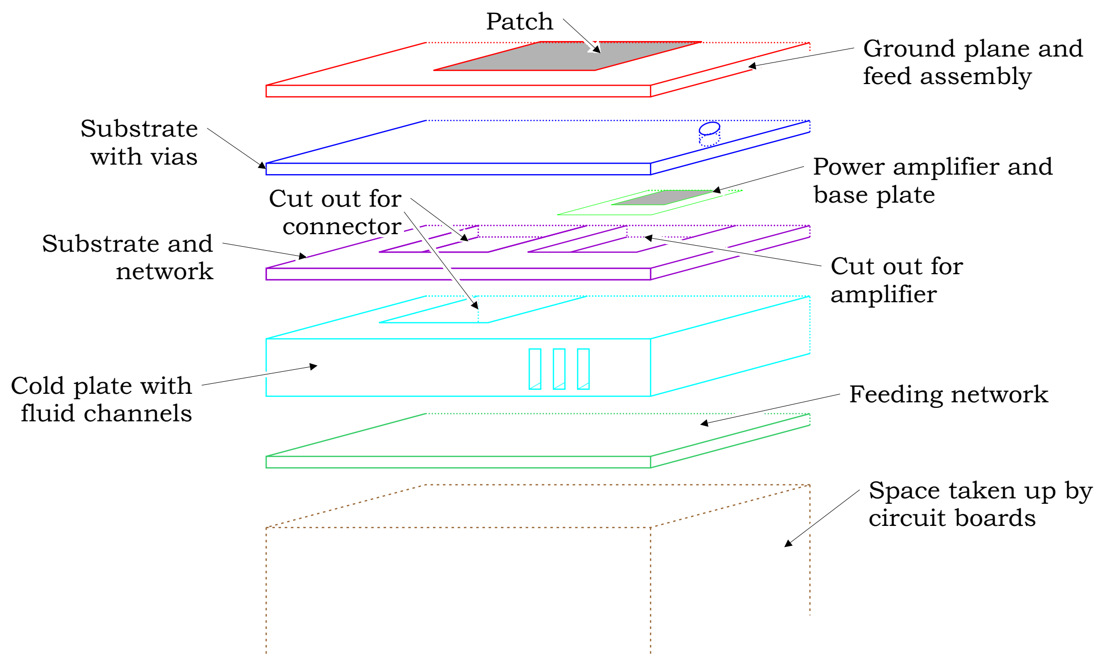

Figure 3.2: Principle layer structure of antenna array (showing just one element).

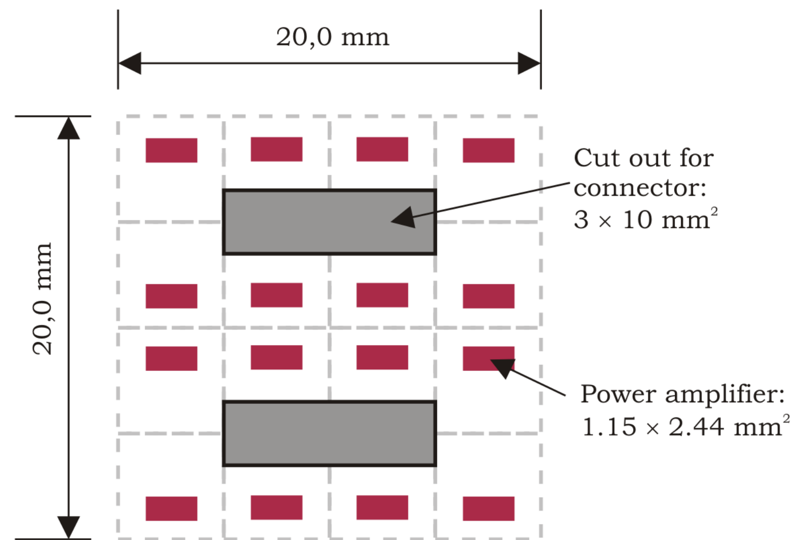

Figure 3.3: Sub-assembly with 4 × 4 elements, top view. The two cut-outs for the connectors restrict the placement of the power amplifiers.

3.2 Environmental conditions

In order to design a cooling system, one has to take the environmental conditions into account. A cooling system for an airborne antenna does have to fulfill other requirements than a cooling system for a vessel. Therefore, special conditions for temperature, pressure, humidity, vibration, acceleration, and orientation have to be taken into account.

Several possible installation locations in an aircraft complicate the specification. A device (including the cooling system) may generally be installed in a temperature and pressure controlled zone as opposed to a non-pressurized and non-controlled temperature location, to name the two extremes. For the first case, the temperature and pressure can be similar to the conditions found at sea-level, whereas the second environment poses special challenges for the cooling system. A more detailed list of installation location categories can be found in [2].

The final location of the antenna array in the aircraft is not known at this stage of the project. However, since the radiating elements of the antenna have to be mounted close to the aircraft skin, a non-pressurized and un-controlled temperature location will be considered as well.

The climatic effects are mainly due to the change in altitude during a flight. Modern commercial planes reach a maximal altitude of approximately 13 000 m (43 000 ft), whereas typical altitudes during a flight are roughly 10 000 m (33 000 ft). This will be taken as a basis for further considerations.

3.2.1 Temperature

According to the International Standard Atmosphere (ISA) as defined by the International Civil Aviation Organization, temperature drops linearly by 6.5 K for every 1000 m rise in altitude up to 11 km. The sea-level temperature is assumed to be 15 °C.

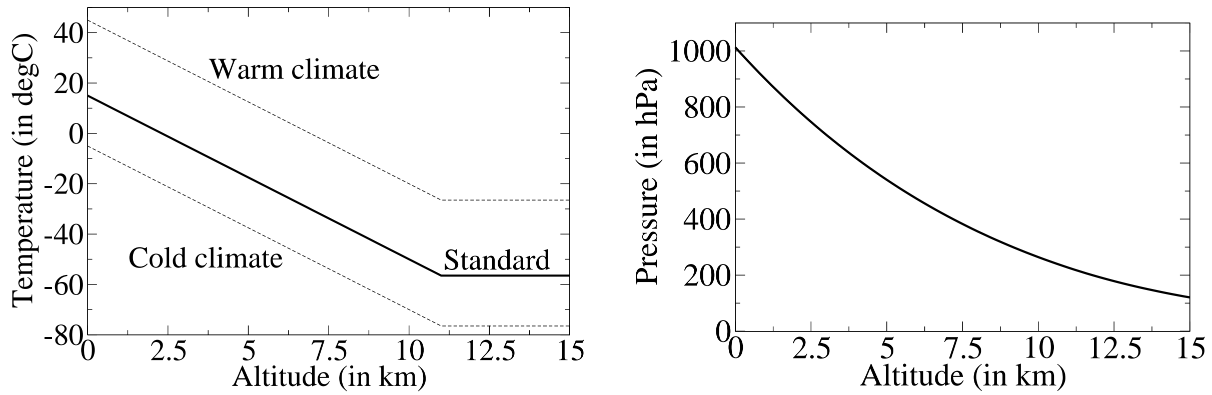

(a) Standard (ISA) and other realistic temperatures over altitude.

(b) Variation of atmospheric pressure with altitude (average sea level pressure is 1013,25 hPa).

Figure 3.4: Temperature and pressure as a function of altitude according to the International Standard Atmosphere (ISA) [3].

Therefore the temperature reaches a value of $-56.5\,°C$ at a height of 11 km where it stays constant up to a hight of 24.5 km (80 000 ft). Of course, this value varies with season and region (see Fig. 3.4(a)), but one can assume a temperature range from $-70\,°C$ to $+45\,°C$ for usual commercial flights [4].

The temperature at the skin of the aircraft is not only influenced by the ambient temperature. It also depends on the speed of the aircraft. This is because a moving fluid experiences a rise in temperature depending on the velocity according to

$$\Delta T = \frac{v^2}{2c} \tag{3.1}$$

where ΔT is the rise in temperature in comparison to the static case, v the velocity and c the specific heat capacity (for air approximately 1000 J/(kg K) [5]) of the medium. At a speed of 900 km/h this results in a temperature rise of roughly 31 K. This temperature has to be added to the ambient temperature to get the resulting temperature at the outer skin of the aircraft.

The temperature rise is significantly more developed for supersonic airliners like the Concord, which was retired in May 2003. The skin temperature for the Concord varied between a value of 127 °C at the nose and 90 °C at the tail for a cruise speed of Mach 2 and an altitude of 17 000 m, for instance [6].

Throughout the remainder of this text a maximal temperature variation from $-70\,°C$ to $+45\,°C$ will be assumed.

3.2.2 Air pressure and density

The correlation between pressure and altitude follows an approximate exponential curve. The correlation is not linear because the density of air decreases with altitude, or in other words, air is compressible. Temperature variations throughout the atmosphere have an effect on pressure as well, which complicates the precise correlation.

The variation of atmospheric pressure with altitude can be seen in Fig. 3.4(b).

For ideal gases (which is a valid assumption here [3]), air density ρ is correlated to air pressure p by

$$\rho = \frac{p}{RT}\,, \tag{3.2}$$

where R is the gas constant for a specific gas.[1] Therefore, air density and pressure are proportional if the temperature variation over altitude is neglected.

3.2.3 Humidity

The ability of the atmosphere to absorb water depends on the temperature and barometric pressure. If either of them is lowered for a saturated atmosphere, the surplus water condenses out as mist.

As an aircraft is exposed to constantly varying relative humidity, temperature, and barometric pressure one has to expect water to condense on components and surfaces in open, unpressurized areas. Appropriate steps (like prohibiting the cooling air to be in direct contact with the electronics) have to be taken to avoid corrosion and leakage currents.

3.2.4 Mechanical conditions

The cooling system of the antenna has not only to operate properly in harsh climatic conditions but also has to withstand mechanical stresses. Vibrations in an aircraft can be significantly higher than for a vessel, and comparatively high acceleration and retardation takes place. Furthermore, the orientation of the antenna with respect to gravitation might influence the cooling system performance as well.

These factors have to be considered and can uniquely determine which cooling system will be used in the final setup. Orientation and acceleration especially effect heat pipes, which are describe in more detail in Sec. 6.5.

3.3 Amplifier

The antenna array consists of many radiating patches, each of which will be fed by a power amplifier operating at a frequency of about 30 GHz. Choosing an appropriate amplifier depends mostly on the following characteristics: operating frequency range, output power, gain, size, and price. TriQuint's gallium arsenide monolithic microwave integrated circuit (GaAs MMIC) power amplifier TGA4509-EPU [7] seems to be the best compromise between all characteristics at this stage of the project.

The characteristics which are important for the thermal management are

- chip dimension (length $\times$ width $\times$ height): 2.44 mm $\times$ 1.15 mm $\times$ 0.1 mm,
- worst case power dissipation: 3.8 W.

The specification of the highest allowable channel temperature is not that straightforward since it directly influences the median lifetime of the device. According to information provided by TriQuint, the median lifetime[2] t_m (in h) for the selected amplifier depends on the channel temperature T_c (in °C) and can be stated as

$$t_m = 3.242 \cdot 10^{-10} \cdot \exp\left(\frac{1.3}{8.6142 \cdot 10^{-5} \cdot (273 + T_c)}\right) . \tag{3.3}$$

[1] R equals 287.05 J K^{-1} kg^{-1} for air [3].

[2] Median lifetime is the time period in which half of a given number of samples fails. The failure criterion is defined here as a 10 % current degradation.

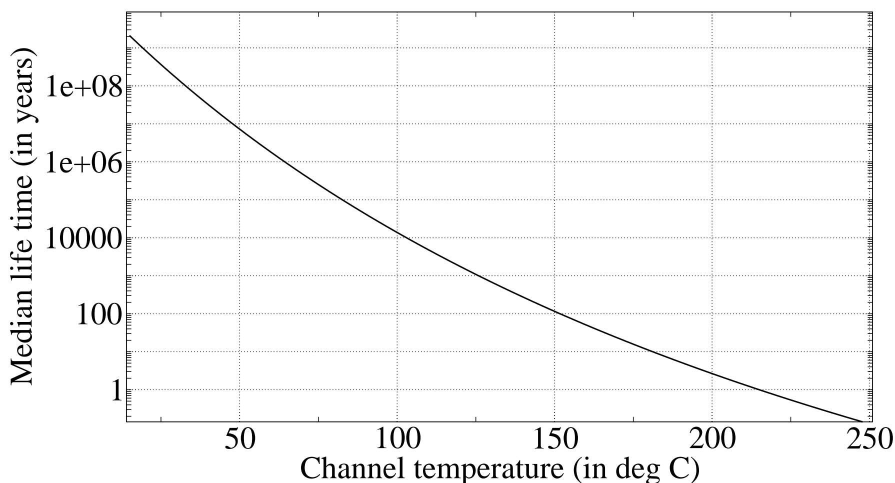

Figure 3.5: Median lifetime of power amplifier TGA4509-EPU depending on channel temperature (see Eq. (3.3)).

The general form of this equation is known as the Arrhenius equation, which describes the rate at which many chemical processes take place. A graphical representation of Eq. (3.3) can be seen in Fig. 3.5. If a maximal channel temperature of 150 °C is assumed, the median lifetime is 115 years. A channel temperature rise of 5 °C results in a median lifetime of 76 years.

The conclusion from Eq. (3.3) is that the highest allowable channel temperature is not a fixed value, and that lower channel temperatures lead to longer median lifetimes. Although a maximal channel temperature of 150 °C is desirable, the amplifier is operated by TriQuint at channel temperatures up to 275 °C for reliability testings.

The amplifier will be used in an active antenna array. If different amplifiers in the array work at different operating points, the resulting antenna beam might be negatively influenced. The operating point depends among other things on the operating temperature. The temperature coefficient of the proposed amplifier is 0.0135 dB/K at the 1 dB compression point for a nominal temperature range of -40 to $+85$ °C. Hence, a temperature difference of 10 K for two given amplifiers results in 0.135 dB (or 3.2 %) difference in gain. This difference is acceptable since it can be compensated by calibration, and a maximal temperature difference between two amplifiers of 10 K will be part of the specification.

Mounting. TriQuint, the amplifier manufacturer, recommends to solder the amplifier to a 0.5 mm thick CuMo (15 %/85 %) base plate to match coefficients of thermal expansion (also see Sec. 3.4). The die should be soldered using an AuSn (80 %/20 %) eutectic solder preform, which has a melting point of 280 °C[3] and provides for good joint strengths [8]. A solder preform is a geometrically well defined piece of solder shaped accordingly to the die dimensions. The MMIC is heated until the solder melts and bonds it to the base plate.

TriQuint's further recommendation is to attach this sub-assembly by means of epoxy or a lower temperature solder to the module floor or housing. Since many amplifiers will be placed closely next to each other, a heat sink will take the place of the housing. TriQuint states that this attachment method leads to an overall thermal resistance

[3] The 30 second mounting temperature of the power amplifier is 320 °C.

Material	200 K	250 K	300 K	350 K	
Aluminum	20.0	21.9	23.2	24.1	[9]
Copper	15.1	16.1	16.8	17.3	[9]
GaAs	5.0	5.5	5.8	6.0	[10]
Iron	10.0	11.0	11.7	12.1	[9]
Kovar			5.0	5.0	[9]
Silver	17.7	18.6	19.2	19.6	[9]
AlSiC (60 % v/v SiC) @ 300 to 450 K: 6.5 to 9.0					[11]
Brass @ 300 to 400 K: 16.9 to 19.7					[9]
CuMo @ 300 to 450 K: 7.0 to 8.0					[12]
CuW @ 300 to 450 K: 6.5 to 8.3					[12]

Table 3.1: Coefficient of thermal expansion α at different temperatures in $10^{-6}K^{-1}$.

of 22.4 K/W between the channel and the housing. Taking the worst case power dissipation of 3.8 W and a median lifetime of 115 years into account, the housing (and therefore the heat sink) temperature should not exceed 65 °C.

3.4 Heat spreader and heat sink materials

Heat dissipating dice are often not directly mounted to the heat sink but first to a heat spreader. Usually one thinks of a head spreader as of a flat plate of material which has ideally a higher thermal conductivity than the material used for the heat sink. The head spreader ensures a more uniform temperature distribution along the die back. Even if the thermal conductivity is not too high, it can become necessary to mount the die not directly to the heat sink. This is due to different coefficients of thermal expansion (CTE) for the semiconductor and the heat sink. Mechanical stresses caused by temperature variations can lead to device failures. Ideally the CTEs of the semiconductor and the heat spreader (or base plate) should be matched to avoid mechanical stresses after mounting. Table 3.1 lists the CTEs of some materials.

Investigations have shown that for GaAs dice AuSn soldered to a heat spreader tensile stresses are much more severe than compressive stresses [13]. Therefore, mounting a GaAs component on Kovar (which has a slightly lower CTE than GaAs) results in failures after several thermal cycles. Soldering the GaAs device on CuMo, AlSiC, and CuW (and therefore on materials with a CTE of up to $10.5 \cdot 10^{-6}$ K^{-1}) did not lead to any failures. The same investigation confirmed that mounting GaAs devices directly on copper (which has a conveniently high thermal conductivity) leads to failures.

According to the manufacturer, a direct adhesive attach of the GaAs MMIC as described in Sec. 3.3 is possible but not recommended. Generally, a thicker adhesive layer will reduce mechanical stresses on the die since it can better counterbalance the different CTEs. On the other hand, one has to consider that from the thermal point of view the adhesive layer should be as thin as possible to reduce thermal resistance. Additionally, thermal resistance of the adhesive is not independent of the number of thermal cycles [14]. Increasing numbers of thermal cycles lead to an increased thermal resistance. While this effect highly depends on the specific adhesive in use, the effect should be taken into account. It is most pronounced for large differences in CTEs of the die and the base plate.

Material	273 K	373 K	
Aluminum	238	230	[9]
AlSiC (60 % v/v SiC)	200	160	[11]
Brass	120		[9]
Copper	400	380	[9]
Iron	82	69	[9]
Silver	418	417	[9]
CuMo @ 300 K: 160 to 170			[12]
CuW @ 300 K: 180 to 200			[12]
GaAs @ 300 K: 54			[15]
Kovar @ 300 K: 11 to 17			[12]

Table 3.2: Thermal conductivity λ in W/(m·K) depending on temperature.

Material	Density in g/cm^3	
Aluminum	2.70	[16]
AlSiC (60 % v/v SiC)	3.0	[11]
Brass (30 % Zn)	8.55	[17]
Copper	8.96	[16]
CuMo	10	[12]
CuW	15.7 to 17.0	[12]
GaAs	5.32	[18]
Iron	7.87	[16]
Kovar	8.1	[12]
Silver	10.45	[16]

Table 3.3: Densities.

Having discussed the coefficient of thermal expansion, another important factor determining the appropriate material is the thermal conductivity λ, which should be as high as possible. The thermal conductivities of some materials are given in Tab. 3.2. As mentioned before, the die can be mounted to the heat sink in two fashions: with or without a base plate (head spreader). As described in more detail in Sec. 4.1, the correlation between plate thickness and thermal resistance is linear. If the thickness of the base plate is small (and values down to 0.1 mm are feasible), the overall thermal resistance can still be small despite lower values of thermal conductivity. The influence of a thin base plate on the overall thermal performance is limited. Since heat sinks are rather large and thick, thermal conductivity becomes a more important factor to reduce the spreading resistance.

Overall weight is important for aerospace applications. Weight can be lessened by reducing system size and by choosing low density materials. The densities of some materials are listed in Tab. 3.3.

Conclusion. If the amplifier is mounted according to the manufacturer's recommendation (as described in Sec. 3.3, also see [19]), the base plate material does not have to match the coefficients of thermal expansion. This allows for discarding special compounds like CuW and CuMo. Thermal conductivity, weight, ease of machining, and price are the remaining major factors.

Copper is the material which has the second highest thermal conductivity (after silver) of all metals. A very good thermal performance can be expected. The only drawback of copper is its high density. Aluminum, whose density is about 30 % of the density of copper, is a good alternative although its thermal conductivity is reduced by 40 % as opposed to copper. Another advantage of aluminum over copper is that it is easier to machine.

Considering the size of the cold plate, it will make up a major part of the antenna. Both copper and aluminum allow mounting of components to the cold plate, which can act as a strong mechanical support.

Copper was chosen to build up a demonstration model, which is described in Sec. 7.1.

4 Heat transfer theory

There are three heat transfer mechanisms to be distinguished: heat conduction, convection, and radiation. Usually more than one mechanism becomes effective at the same time, but it is convenient to analyze and describe each of them separately.

4.1 Heat conduction

Thermal conduction works without the transport of a medium by means of atomic and molecular interaction. Heat conduction occurs in solid, liquid, and gaseous media whenever a temperature gradient occurs. The correlation between the heat flux density vector $\dot{\mathbf{q}}$ and the temperature gradient was stated by Fourier as [20]

$$\dot{\mathbf{q}} = -\lambda \nabla T \,, \tag{4.1}$$

where λ is the thermal conductivity and T the temperature. The negative sign in Eq. (4.1) states that heat always flows from hot to cold regions. The thermal conductivity λ depends on temperature and pressure. Anisotropic media (e. g. wood) exist, but for all materials which are being considered throughout this text λ is a scalar since these materials are isotropic.

For most cases Eq. (4.1) cannot be solved directly because the temperature distribution changes due to heat transfer. Heat conduction can generally be described by Fourier's partial differential equation

$$\frac{\partial T}{\partial t} = a \nabla^2 T \,, \tag{4.2}$$

where t is the time and a the thermal diffusivity [20]. The thermal diffusivity depends uniquely on material properties and is given as

$$a = \frac{\lambda}{\rho c} \,, \tag{4.3}$$

where λ is the thermal conductivity, ρ the density, and c the specific heat capacity.

In the special *static* case the temperature gradients do not depend upon time. The antenna array will be used in an aircraft, where ambient temperature changes at all moments can be assumed to be slow as opposed to the reaction time of the system. Then for each moment the system can be said to be in a static (or quasi-static) state, and Eq. (4.2) simplifies to

$$0 = \nabla^2 T \,. \tag{4.4}$$

If the temperature distribution just depends on one variable (which is the case for a plane wall), namely x, Eq. (4.4) can be further simplified to

$$0 = \frac{\mathrm{d}^2 T}{\mathrm{d}x^2} \,. \tag{4.5}$$

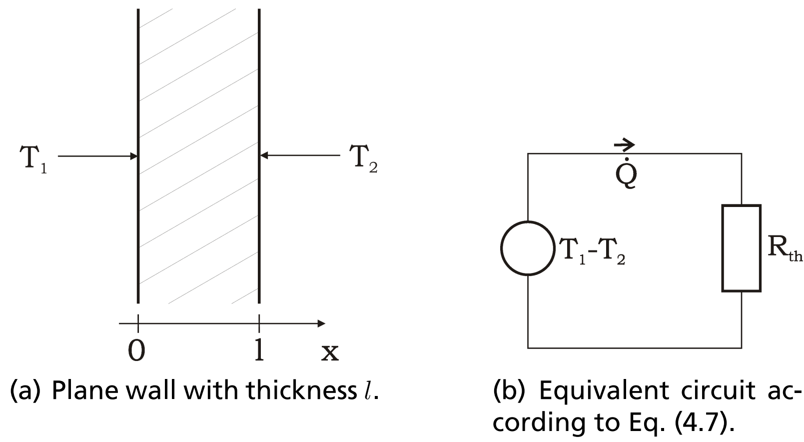

(a) Plane wall with thickness l.

(b) Equivalent circuit according to Eq. (4.7).

Figure 4.1: Steady state thermal conduction.

The last equation can be solved by integration and it results in

$$T(x) = c_1 x + c_2 \,. \tag{4.6}$$

If the temperatures at the wall boundaries are given as $T_1 = T(x = 0)$ and $T_2 = T(x = l)$ as shown in Fig. 4.1(a), Eq. (4.1) can be rewritten as

$$\dot{Q} = \lambda \frac{A}{l}(T_1 - T_2) = \frac{T_1 - T_2}{R_{\text{th}}} \,, \tag{4.7}$$

where $\dot{Q}$ is the heat flux. This equation is known as the equation of static heat conduction. The thermal resistance R_{th} for a plane wall is given as

$$R_{\text{th}} = \frac{l}{\lambda A} \,. \tag{4.8}$$

In analogy to steady currents in electrodynamics, statical thermal problems can now be depicted and analyzed with the same tools and techniques which are common in electrical engineering. Ohm's law in electrodynamics corresponds to Eq. (4.7) in thermodynamics; the electrical current corresponds to the thermal current $\dot{Q}$, the potential difference to the temperature difference $T_1 - T_2$, and the electrical resistance to the thermal resistance R_{th}. Figure 4.1(b) shows the equivalent thermal circuit of the aforementioned steady case. Using Kirchhoff's laws, equivalent thermal resistances can be found for more complicated problems consisting of several plates. The configuration can be depicted in schematic diagrams which are often used in electrical engineering.

The thermal conductivity λ of metals is due to two approximately independent factors: lattice vibrations and movement of electrons. This can be summarized as [21]

$$\lambda = \lambda_e + \lambda_l \,. \tag{4.9}$$

Thermal conductivity due to electron movements λ_e dominates for metals and correlates to electrical conductivity by

$$\lambda_e = L_c \sigma T \,, \tag{4.10}$$

where σ is the electrical conductivity and L_c is the Lorenz constant given as $2.45 \cdot 10^{-8}\ \text{V}^2\text{K}^{-2}$ [21].

4.2 Convection

As opposed to heat conduction, convective heat transfer is due to a moving fluid, i. e. gas or liquid. Generally, one distinguishes between *natural* and *forced* convection. The fluid moves without any additionally applied force for natural convection, and fluid flow is imposed by by a pump, fan, or other machinery for forced convection. In the following section the special case of heat transfer between a solid and a fluid will be presented.

The mathematical analysis of convective heat transfer involves the solution of a coupled set of partial differential equations to describe the temperature, velocity, and pressure fields. The vector velocity field results from the Navier-Stokes equations, which states the balance of forces for an infinitesimal element of an uncompressible fluid [22]. A general analytical solution has not been found and analytical solutions only exist for special cases. Numerical simulations can be used to approximate a solution.

The convective heat transfer between an isothermal surface and a fluid is empirically described in Newton's law of cooling

$$\dot{q} = h(T_w - T_\infty)\,, \tag{4.11}$$

where T_w is the plate temperature and T_∞ the homogeneous temperature of the surrounding fluid. The heat transfer coefficient h describes the interface between the surface and the fluid. It depends on the heat sink geometry as well as on fluid and flow properties. The thermal resistance is given as [5]

$$R_{\text{th}} = \frac{1}{hA}\,. \tag{4.12}$$

If the fluid temperature is assumed to vary along the surface A, which is the case for heat exchangers, the temperature difference in Eq. (4.11) has to be replaced by a logarithmic temperature difference [23]

$$\Delta T_{\log} = \frac{T_o - T_i}{\ln \frac{T_w - T_i}{T_w - T_o}}\,, \tag{4.13}$$

where T_i and T_o are the fluid inlet and outlet temperatures, respectively.

Usually two fluid flows are distinguished: laminar and turbulent. Turbulent flow differs from laminar flow as fluid movement in each point is not along one direction. In the eyes of an observer, turbulent flow is complicated and random. Heat transfer depends on the flow type.

4.2.1 Dynamical similarity and dimensionless numbers.

Fluid flow and convective heat transfer are often described by means of dimensionless numbers in order to generalize once found results and correlations. The approach is to assert the similarity of two different flows or heat transfer situations. Two different flows are called similar if there is a constant ratio between geometrical and physical properties for every two congruent points.

Some of these numbers are introduced in the following paragraphs.

Reynolds number. The dimensionless Reynolds number characterizes the flow condition. For low Reynolds numbers laminar flow results whereas for numbers above a critical value turbulent flow exists. For circular pipes, the Reynolds number Re is given as

$$Re = \frac{vd}{\nu} \tag{4.14}$$

where v is the fluid velocity, d the pipe diameter, and ν the fuild's kinematic viscosity. The Reynolds number can also be interpreted as the ratio

$$Re = \frac{\text{Inertia forces}}{\text{Viscous forces}} .$$

Inertia forces describe the fluid's natural resistance to acceleration whereas viscous forces are due to internal friction of the fluid.

The kinematic viscosity ν is a function of density ρ and dynamic viscosity η,

$$\nu = \frac{\eta}{\rho} . \tag{4.15}$$

The critical Reynolds number for pipes below which laminar flow exists is 2300 [23]. For $2300 < Re < 10^4$, the flow is considered to be unstable. Fully turbulent flow is assumed for Reynolds numbers above 10^4.

Non-circular pipe geometries can be calculated by using the hydraulic diameter d_h instead of the circular diameter in Eq. (4.14). The hydraulic diameter is given as

$$d_h = 4\frac{A}{U} , \tag{4.16}$$

where A is the cross-sectional area and U the wetted perimeter [24]. It is apparent that the hydraulic diameter for pipes with quadratic cross sections equals the side length.

Nusselt number. The dimensionless Nusselt[1] number describes the improved heat transfer from a surface to a fluid due to convection in contrast to the heat transfer based solely on conduction. It is also called the dimensionless heat transfer coefficient and is given as

$$Nu = \frac{hL}{\lambda} , \tag{4.17}$$

where h is the heat transfer coefficient, L a characteristic length, and λ the thermal conductivity of the fluid. The characteristic length for a flat wall is the distance from the wall edge; the characteristic length of a pipe is the hydraulic pipe diameter.

Prandtl number. The Prandtl number is uniquely based on material properties and equals the ratio of the fluid viscosity and thermal diffusivity

$$Pr = \frac{\nu}{a} . \tag{4.18}$$

Low numbers indicate that heat transfer is dominated by conduction while convective heat transfer is described by high numbers.

The Prandtl number of dry air for temperatures from 0 °C to 100 °C is roughly 0.71; for water at 98,1 kPa it ranges from 13.67 at 0 °C over 5.43 at 30 °C down to 1.75 at 100 °C [23].

[1] Wilhelm Nusselt was a German engineer who graduated 1904 from the Technical University Berlin. Later on he worked as a professor at the universities in Karlsruhe and Munich [25].

4.2.2 Natural convection

Natural (or free) convection is caused by buoyancy of a fluid in the earth's gravitational field. The buoyancy is caused by pressure differences, which are due to temperature gradients.

Heat transfer by free convection (especially with air as the working fluid) would be often desirable since no additional appliance has to be installed and maintained. However, heat transfer by means of free convection can usually be just considered for small amounts of dissipated heat. Since gravitation plays an important role in free convection heat sinks, the orientation of the heat sink becomes important as well.

If a natural convection heat sink is operated in an unpressurized area in an aircraft, pressure and temperature changes due to altitude variations during the flight have to be taken into account.

Empirical solutions based on dimensionless numbers for heat transfer by natural convection have been presented in the literature [20, 23, 26]. As an example, results for a horizontal flat isothermal plate will be presented in Sec. 6.1.

4.2.3 Forced convection

Fluid flow for forced convection is initiated by some kind of machinery like a pump, fan, or blower to name a few. Natural convection can be neglected in most cases when analysing forced convection fluid flow.

Although different schemes for heat transfer by means of forced convection are conceivable, the focus will be on heat transfer from a solid wall (like a pipe wall) to a fluid. The most simple case is a flow parallel to a flat wall. The flow will be influenced by the wall due to the fluid friction, which is described by fluid viscosity. Directly at the boundary, the velocity decreases to zero. The flow velocity approaches the initial velocity (which occurred before the plate was entered) a certain distance away from the boundary, see Fig. 4.2(a). This boundary layer thickness is denoted δ. If the wall has a different temperature than the fluid, a temperature boundary layer with thickness δ_T exists. For liquids ($Pr > 1$), it yields that $\delta_T < \delta$ [23].

If one simplifying assumes that the heat transfer in the temperature boundary layer is solely based on conduction, Eqs. (4.7) and (4.11) lead to

$$h = \frac{\lambda}{\delta_T} \, . \tag{4.19}$$

Therefore, in order to assess the heat transfer from a surface, one has to know the fluid's thermal conductivity and the thermal boundary layer thickness. The Nusselt number in Eq. (4.15) can now be expressed as

$$Nu = \frac{L}{\delta_T} \, . \tag{4.20}$$

Boundary layers exist as well in pipe flow, which is more relevant in this context than flow along a wall. Pipe flow occurs in liquid cold plates, for instance. It will be described in more detail in the following paragraphs.

Laminar pipe flow. The velocity and temperature profiles for laminar pipe flow are parabolic [23]. They are exemplary shown in Fig. 4.2(b). The Nusselt number (and

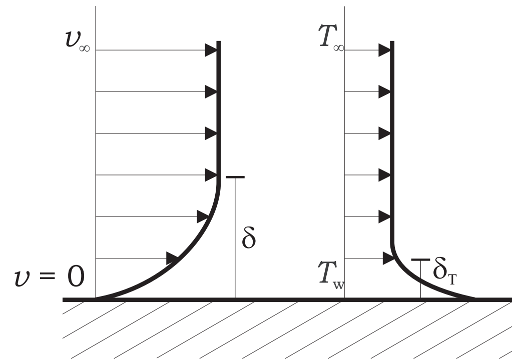

(a) Flow along wall, fluid is a liquid ($\delta_T < \delta$), after [23].

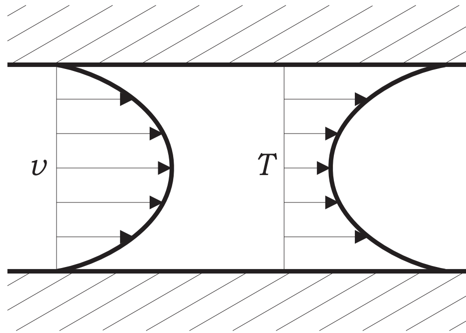

(b) Laminar flow through pipe, after [23].

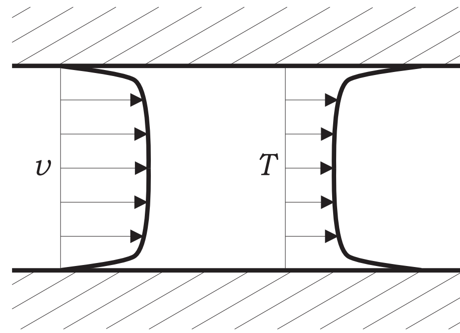

(c) Turbulent flow through pipe, after [27, 24].

Figure 4.2: Velocity and temperature profiles for fully developed flows. The wall temperature is higher than the fluid temperature.

therefore the heat transfer coefficient h) can be analytically found. It is given as [28]

$$Nu = \begin{cases} 4.36 & \text{for constant heat flux density along the wall} \\ 3.66 & \text{for constant temperature along the wall.} \end{cases} \tag{4.21}$$

It has to be noted that the heat transfer coefficient does not depend on fluid velocity for laminar flow. Wall roughness has no influence on heat transfer.

Turbulent pipe flow. As opposed to laminar flow, turbulent flow cannot be analytically described. Equations are therefore based on experiments, and stated functions differ in literature.

The velocity and temperature profiles of fully-developed turbulent flow are shown in Fig. 4.2(c). It can be seen that both the velocity and the temperature are nearly constant in the center of the pipe. In the region close to the walls, laminar flow exists. This explains the higher temperature difference close to the walls.

For fully-developed turbulent flow in a circular duct, the Nusselt number can be approximated as [23]

$$Nu \approx 0.0235 \cdot Re^{0.8} \cdot Pr^{0.48} \tag{4.22}$$

for $10^4 < Re < 10^6$ and $0.6 < Pr < 50$. Wall roughness (as described by the drag coefficient) influences heat transfer; the rougher the wall, the better the heat transfer. Equation (4.22) is valid for smooth walls and defines a lower boundary for the Nusselt number.

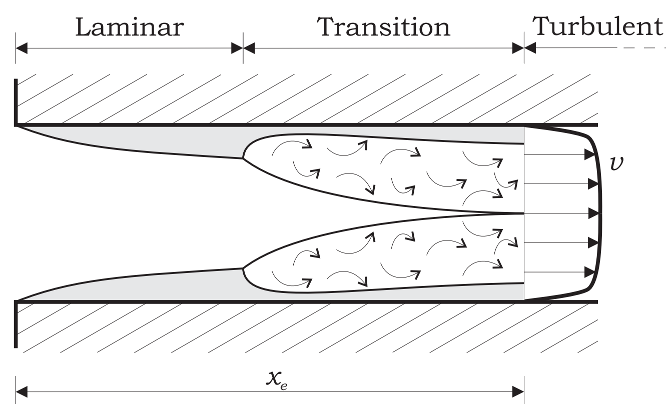

Figure 4.3: Entrance region for turbulent flow, after [23].

Heat transfer is immensely improved for turbulent flow as opposed to the laminar flow case. A simple numerical example for water shows this. Fully turbulent flow is assumed to occur for Reynolds numbers above 10^4. The Prandlt number for water at 50 °C is 3.57 [23]. It follows after Eq. (4.22) that $Nu = 84$ for turbulent flow, whereas the Nusselt number for laminar flow as given in Eq. (4.21) is significantly lower. Therefore, turbulent flow is the preferred flow type for heat exchangers, which comes at a cost of a higher flow resistance so that more powerful pumps have to be utilized.

Entrance region. If a fluid enters a heated pipe, it takes a certain distance until the velocity profiles (as shown in Figs. 4.2(b) and 4.2(c)) are fully developed. This region is called the hydrodynamic entrance region, and its length is denoted as x_e. For flows approaching both the laminar and turbulent case, the flow near the walls after the entrance is laminar. For turbulent flow, turbulent components first occur after a certain length as shown in Fig. 4.3. This transitional region is followed by the region of fully-developed turbulent flow.

For laminar flow, the hydrodynamic entrance region x_e is given as [28]

$$x_e = 0.056 \cdot Re \cdot d \, . \tag{4.23}$$

For non-circular pipes, the pipe diameter d has to be substituted with the hydraulic diameter according to Eq. (4.16).

The entrance region for turbulent flow is short in comparison to the laminar flow case due to the better mixing of the fluid. It is given as [28]

$$10 \leq \frac{x_e}{d} < 60 \, . \tag{4.24}$$

Since turbulent flow is desirable for most heat exchanger configurations, one can consider to increase the pipe length at the entrance by x_e. This would result in an already developed turbulent velocity profile when the flow reaches the heated region. This would mean that a high heat transfer is ensured for the whole heated pipe surface.

Fin efficiency. Fins are often used to increase the convective heat transfer by increasing the contact area between the solid and the fluid. The heat transfer does not increase proportionally with the contact area since the temperature from the base to the tip of

the fin decreases due to the limited thermal conductivity of the material. The fin efficiency factor describes the heat flow of an actual fin to the theoretical heat flow of an isothermal fin.

4.3 Thermal radiation

As opposed to heat conductance and convection, no additional medium is necessary for heat transfer by means of electromagnetic radiation. Although every object with a temperature above absolute zero emits thermal radiation, the spectrum and power depends on the object's properties and its absolute temperature. Even slight changes in the surface properties of an object can highly influence the thermal radiation. In order to simplify the analysis, one consideres a special kind of radiating object, a blackbody.

A blackbody is a hypothetical object which is able to absorb all incident radiation. Since Kirchoff's law of radiation states that the emissivity of an object is equal to its absorbance at the same temperature, a blackbody also emits maximal thermal radiation. The power P emitted by a blackbody is given by the Stefan-Boltzmann law

$$P = \sigma A T^4 \,, \tag{4.25}$$

where σ is the Stefan-Boltzmann constant given as $5.67 \cdot 10^{-8}$ $\mathrm{Js^{-1}m^{-2}K^{-4}}$, A the total radiating area, and T the absolute temperature.

Example. The maximal possible radiated energy from an antenna element can be assessed even if no specific surface shall be assumed at this point. This is possible if one assumes the antenna element to be a blackbody.

The antenna element under consideration consists of a quadratic ground plate with an edge length of 5 mm. Mounted on one side of the ground plate is the heat dissipating amplifier. Since many antenna elements will be mounted directly next to each other, no radiation can occur to the sides of most of the antenna elements. Therefore, radiation to the sides will be neglected here. Two radiating surfaces per element are remaining, the top and bottom surfaces.

If one assumes that the amplifier has a temperature of 100 °C and using Eq. (4.25), each (blackbody) surface radiates a power of 27.5 mW. This totals to 1.45 % of the formerly assumed 3.8 W maximal power dissipated by the amplifier.

Considering that a real body with a less than ideal surface will radiate even less energy, it becomes apparent that the heat dissipated by the amplifier cannot be transfered by means of radiation.

Due to the small portion of power which is being radiated as opposed to the power being dissipated by the amplifier, thermal radiation will be neglected in the remainder of this text.

5 Software

Numerical simulations are one possibility to approach problems in thermal and fluid dynamics. Several advantages and shortcomings arise.

The governing equations of thermodynamics, as described in Sec. 4, cannot generally be solved. While empirical equations exist to describe certain simple geometries, and analytical solutions were found for special cases [22], numerical simulations offer a generalized approach to approximate solutions for any given geometry. Numerical simulations are advantageous when numerical models can be build with less practical and financial strains than real-world prototypes. This is especially true for environments in which prototypes cannot easily be examined, namely low or high temperatures and altitudes. Furthermore, numerical models can usually be modified with relative ease and allow for a quick optimization. Early rough numerical models can highlight future problematic aspects of a design and can speed up the optimization process.

On the other hand, numerical simulations are always based on certain assumptions concerning boundary conditions and material properties. Wrong or imprecise assumptions can easily lead to erroneous solutions, and great care has to be taken at this stage of the simulation. Although measurement uncertainties do not exist in numerical simulations, the overall solution is just an approximation of the real world situation. This is due to the fact that the solution domain is somehow discretized, and the solution depends on the discretization. While finer grids can introduce new problems, they usually lead to more precise solutions. The drawback is an increase in computer and time resources. Therefore, a compromise has to be found.

In the following two sections, the commercial software packages Flotherm[1] and Thermal Desktop[2] (utilizing Sinda/Fluint) will be presented. It will be highlighted why Flotherm was chosen to conduct numerical simulations for this project.

5.1 Thermal Desktop

Thermal Desktop is a CAD based thermal modeling software [29]. The software describes a given geometry as a network of lumps and solves it using the thermal and fluid network solver Sinda/Fluint. For the one-dimensional steady state case, the network representation would look similar to Fig. 4.1(b) on p. 16. In order to simulate transient cases, further elements, which would be called capacitors in the electrodynamics equivalent, are added.

Convective heat transfer and fluid flows are treated empirically. The software makes

[1]FLOTHERM® is a registered trademark of Flomerics Ltd.

[2]Thermal Desktop® is a registered trademark of Cullimore & Ring Technologies, Inc.

use of the dimensionless numbers as described in Sec. 4.2.1. This approach leads to fast results as opposed to computational fluid dynamics (CFD) calculations [30]. However, the empirical approach is its major drawback since assumptions have to be made to be able to apply the empirical formulas. For instance, convection is limited to cases with vertically or horizontally aligned walls, and flows are assumed to be fully developed.

A thermal network representation is well suited to one-dimensional problems. A piping loop is one example, or geometries with thin walls. Thin means in this case that the wall can be assumed isothermal. Whenever thermal distributions *inside* a wall become important, as it is the case for heat spreaders, a full discretization of the solution domain is better suited. The same is true for arbitrary flows, which cannot be described empirically.

5.2 Flotherm

Flotherm [31] is based on computational fluid dynamics to compute heat transfer for heat conduction, forced, and free convection, and radiation. Its main advantage is the possibility to predict fluid flows, both laminar and turbulent. As opposed to Thermal Desktop, splitting flows as well as flows around obstacles like fins can be modeled. This comes at a cost of an increased demand for time and computer resources.

Instead of representing a geometry as a thermal network, the whole solution domain is being discretized on a Cartesian mesh. The governing differential equations, which are partly described in Sec. 4, are being solved directly. No additional assumptions have to be made in order to get an approximate solution.

Several sources of error in modeling a given geometry exist. Since a Cartesian grid is used, only rectangular geometries can be modeled precisely. Oblique, bent, and curved surfaces have to be approximated by many cubes or prisms, for instance. Although material properties can be accurately specified, they are often not exactly known. Initial assumptions can often be rough, which is another reason for an imprecise solution.

Defining an appropriate grid is one of the main challenges in using the software. Whereas a rough grid leads to fast computations, a fine grid is necessary to model areas with high temperature, pressure, and velocity gradients. Generally, a finer grid leads to better accuracy. The grid does not have to be uniform, and several tools exist to simplify grid definition. For instance, the grid can be refined just locally in areas which are assumed to contain high gradients or which are of special importance. The overall accuracy in comparison to a non-localized grid is being preserved [32]. Cells with large aspect ratios and large changes in cell dimensions of adjacent cells should be avoided. Smoothing algorithms help to achieve this.

It became apparent that Flotherm should be chosen for this project. This allows arbitrary fluid flows to be calculated, which occurred at the fluid inlets, for instance.

6 Cooling techniques

Several cooling techniques are available. Some cooling techniques, ordered roughly by increasing cooling effectiveness and complexity, are:

1. Natural convection air cooling
2. Forced convection air cooling
3. Cooling utilizing heat pipes
4. Liquid cold plates
5. Micro-channel liquid cold plates

Each technique offers advantages and disadvantages, which define the final choice. Often more than one choice is feasible, but for most commercial cases the least complex solution is used since it usually involves the lowest costs. Deviation from this rule occurs when costs play a minor role. Weight and reliability, for instance, are important for space- and airborne applications.

6.1 Natural convection air cooling

The following two examples will demonstrate that a heat sink based on natural convection does not provide the necessary cooling effectiveness for the antenna array under consideration.

Empirical formulas will be used, which limit the analysis to some specific geometries. Here, a horizontal flat isothermal plate will be taken as the heat source. The coefficient which has to be determined is the heat transfer coefficient h. Once it has been obtained, the convective heat flux density $\dot{q}$ can be determined by Eq. (4.11). The heat transfer coefficient can be determined by finding the dimensionless Nusselt number according to Eq. (4.17),

$$Nu = \frac{hL}{\lambda}\,, \tag{6.1}$$

where L is the heated plate area divided by the plate circumference and λ the thermal conductivity of the fluid. For a horizontal, flat plate the Nusselt number is also given as [20]

$$Nu = \begin{cases} 0.766[Raf(Pr)]^{1/5} & \text{for } Raf(Pr) < 7 \cdot 10^4 \text{ (laminar flow)} \\ 0.15[Raf(Pr)]^{1/3} & \text{for } Raf(Pr) > 7 \cdot 10^4 \text{ (turbulent flow)} \end{cases} \tag{6.2}$$

with

$$f(Pr) = [1 + (0.322/Pr)^{11/20}]^{-20/11}\,, \tag{6.3}$$

where Ra and Pr are the dimensionless Rayleigh and Prandtl numbers, respectively.

For the first example, an array of 100×100 array elements is assumed. Each square element has a side length of 5 mm and dissipates 3.8 W. This results in an antenna array size of 0.25 m^2 and the worst case dissipated power totals to 38 kW. The ambient air is assumed to be at $T_\infty = 20$ °C. If the maximal plate temperature is taken as $T_w = 70$ °C, allowing for a temperature difference of 50 °C, the flow is turbulent and the heat transfer coefficient is $h = 4.75$ Wm^{-2}K^{-1}. According to Eq. (4.11) the total heat flux is only 60 W, which is about 0.16 % of the total dissipated power in the antenna. This result underlines that cooling by means of natural convection in air is not sufficient, and it does not even add significantly to the overall required heat flux.

In the second numerical example an array size of four by four elements (4 cm^2) will be assumed. This conforms to a configuration which might be build as a demonstration model later on in the ATENAA project. The cooling would be improved by simply increasing the size of the horizontal base plate, which will be assumed to be isothermal here (neglecting the finite thermal conductivity of the plate). In order to transfer $4^2 \cdot$ 3.8 W of dissipated power, the square plate would have to have a size of 0.256 m^2 or a side length of 50.6 cm.

The results of the second example were verified by numerical simulations utilizing Flotherm. A 1 cm thick copper plate was used as the heat spreader, and the assumption of a nearly isothermal surface was confirmed.

Conclusion. Simple numerical examples showed that cooling based on natural convection is not feasible for the antenna array. Choosing a cooling technique other than natural convection helps to avoid the following problems as well: The heat would have had to be transferred to the sides of the array first since a fin heat sink cannot be directly implemented where power is dissipated due to assembly constraints as described in Sec. 3.1. Furthermore, the performance of a possible fin heat sink depends on air density as well as on orientation with respect to the gravitational field. The system would have had to be designed for the worst case, which would further increase overall weight and size.

6.2 Forced air cooling

Air cooling by means of forced convection is realized by air moving devices like fans and blowers. Forced air cooling is a very common choice for many applications since a cooling system is often low-cost and can comparably easily be build. In an aircraft, basically two environments for forced air cooling are conceivable: the pressurized and controlled temperature zone and the non-pressurized and non-controlled temperature zone. Altitude significantly affects the second environment. The first scenario, a temperature and pressure controlled location for the heat sink, simplifies overall design since different ambient conditions do not have to be taken into account. Since the final location of the heat sink in the aircraft has not been decided yet at this stage of the project, the more general second scenario will be characterized in the following.

The cooling air from outside the aircraft is often conditioned before it is passed further on to the cooling system. This step is necessary to filter out humidity, dust, and grease particles. Although this greatly reduces the amount of humidity, humidity might nevertheless pass on and accumulate on electronic equipment. The humidity

can lead to failures, and therefore direct contact of cooling air with electronics should be avoided [26]. This greatly influences the basic design of the cooling system.

One way of collecting fresh air can be by means of an inlet in the outer skin of the aircraft. This ram air can actually be a heat source rather than a coolant. Referring to Sec. 3.2.1, the ambient temperature on a warm day can be 45 °C. The temperature increase for a typical cruise speed (900 km/h) is approximately 31 K, according to Eq. (3.1). Adding these two numbers up (and neglecting that the cruise speed does not occur at ground-level) leads to an inlet temperature of 76 °C, which is already above the maximal heat sink temperature of 65 °C for the amplifier under consideration (see Sec. 3.3). Therefore, the air pre-conditioning has to include cooling. Different sections of the airplane (passenger cabin, electronics) require different temperatures and pressures. The system regulating the on-board climate is often referred to as the environmental control system (ECS). The air source is often bleed air from the aircraft's engine compressor stage at a temperature of 300 °C. Air temperatures below 0 °C are nevertheless available [33]. A simple cooling system based on evaporating a controlled amount of water shortly after the ram air intake is presented in [34], which can be used for pods being not connected to the ECS, for instance.

The interesting figure in determining the performance of an air cooling system is the temperature difference between the air inlet and the heat sink hot spot. The temperature rise is due to two factors:

- ΔT_A describes the temperature rise of the cooling air as it passes through the heat sink.
- ΔT_B is due to the thermal resistance described by the heat transfer coefficient between the surface and the moving fluid.

Therefore, the hot spot surface temperature T_s is given as [26]

$$T_s = T_{\text{in}} + \Delta T_A + \Delta T_B \,, \tag{6.4}$$

where T_{in} is the air inlet temperature.

Summand ΔT_A. First, the temperature rise ΔT_A will be discussed; a good introduction to fan heat sinks is given in [26, 35]. The first step in determining a fan for a forced air cooling is to assess the required volumetric fluid flow rate. It depends on the specific heat of the fluid. Specific heat c, which is also called specific heat capacity, is the amount of heat required to change one kilogram of a substance by one kelvin. This quantity becomes important if one wants to assess the amount of fluid required to ensure a defined maximal temperature difference between the fluid inlet and outlet, here denoted as ΔT_A. The following equation results from taking the derivative with respect to time of the defining equation for specific heat

$$\dot{Q} = c\dot{m}\Delta T_A \,, \tag{6.5}$$

where $\dot{Q}$ is the heat flux, c the specific heat capacity, $\dot{m}$ the mass flow rate, and ΔT_A the temperature difference between the outlet and inlet. The mass flow rate can be expressed as

$$\dot{m} = \rho G \,, \tag{6.6}$$

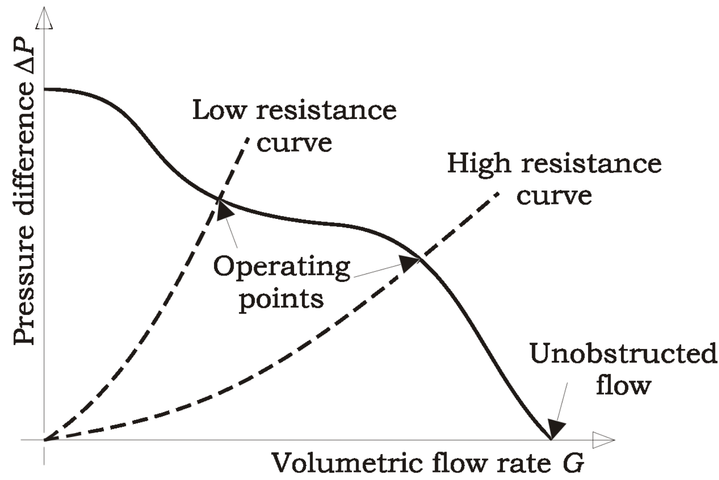

Figure 6.1: Typical fan performance curve. The intersection between the system resistance curve (dashed) and the fan performance curve defines the operating point.

where G is the volumetric flow rate. Therefore, the mass flow rate is directly proportional to density. Now the required volumetric flow rate for a given heat flux and maximal temperature difference is given as

$$G = \frac{\dot{Q}}{c\rho\Delta T}\,. \tag{6.7}$$

The volumetric flow rate is not the only characteristic property of fans. A fan can only provide a certain pressure drop between the inlet and outlet side of the fan. A fan's performance can be depicted in a fan performance curve, which correlates the volumetric flow rate and the pressure drop. A typical fan performance curve can be seen in Fig. 6.1. It states that a fan can deliver a high volume flow rate if the airflow is not obstructed. The airflow can shut off for high flow resistances.

The flow resistance is determined by the system, since the air will have to flow around and through components including heat sinks and filters. The system resistance is a measure of required pressure drop for a given volumetric flow rate. The pressure drop as a function of volumetric flow rate can be expressed as [36]

$$\begin{aligned} \Delta p &= k_l G && \text{for laminar flow,} \\ \Delta p &= k_t \rho G^2 && \text{for turbulent flow,} \end{aligned} \tag{6.8}$$

where k_l and k_t are system specific constants for the laminar and turbulent case, respectively. The operating point of the fan is determined by the intersection of the fan performance and system resistance curve (as shown in Fig. 6.1). Once the resistance curve is known, an appropriate fan can be chosen.

The resistance curve can be derived by

- using empirical formulas (for rather simple geometries),
- measurement of the real system, or
- simulation of the given geometry based on computational fluid dynamics.

The last approach will be used in Sec. 6.2.2.

Air filters are often necessary to clear the cooling air from dust particles and other impurities. A filter can significantly increase the system resistance. In order to minimize the pressure drop across the filter, the filter surface area should be as large as possible.

Summand ΔT_B. The second characteristic number in Eq. (6.4), ΔT_B, is governed by Eq. (4.11). The heat transfer coefficient can be determined by empirical formulas for specific geometries involving dimensionless numbers as defined in Sec. 4.2.1. Assumptions about flow conditions (e. g. fully developed flow) and a limited amount of available formulas in the literature for different geometries restrict this approach. For arbitrary geometries and different flow conditions, numerical simulations are used to determine ΔT_B.

6.2.1 Influence of altitude

The influence of altitude on air cooling has been presented in [26, 36, 37].

Influcence on ΔT_A. Since the mass of air and not the volume governs the cooling (see Eq. (6.5)), the air density decrease with altitude (as described in Sec. 3.2.2) reduces the cooling effectiveness. In other words, the temperature difference between fluid inlet and fluid outlet increases according to

$$\Delta T_a = \frac{\rho_0}{\rho_a} \Delta T_0 \,, \tag{6.9}$$

where index 0 indicates the nominal condition at sea level and a the altitude condition. Therefore, the temperature rise is inversely proportional to the air density.

In order to describe the fan performance depending on altitude, so-called *fan laws* can be used. They assume constant fan efficiency[1] at all operating points and altitudes and can be stated as [36]

$$G_a = G_0 \cdot \frac{\omega_a}{\omega_0} \tag{6.10}$$

$$\Delta p_a = \Delta p_0 \cdot \left(\frac{\omega_a}{\omega_0}\right)^2 \cdot \frac{\rho_a}{\rho_o} \tag{6.11}$$

$$P_a = P_0 \cdot \left(\frac{\omega_a}{\omega_0}\right)^3 \cdot \frac{\rho_a}{\rho_o} \tag{6.12}$$

where:

G volumetric flow rate ($\mathrm{m^3/s}$);
Δp pressure drop ($\mathrm{N/m^2}$);
P fan power (W);
ω revolutions per minute;
ρ density of air ($\mathrm{kg/m^3}$);
$\diamondsuit_a$ index for condition at specific altitude;
$\diamondsuit_0$ index for nominal condition.

It can be seen that the volumetric flow rate G is independent of air density, whereas the pressure drop and fan input power are directly proportional to density.

[1] Fan efficiency is defined as the ratio between useful output power (moving air) and fan input power.

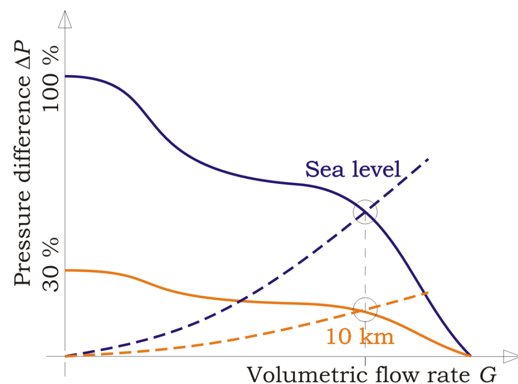

(a) Constant speed fan for turbulent flow.

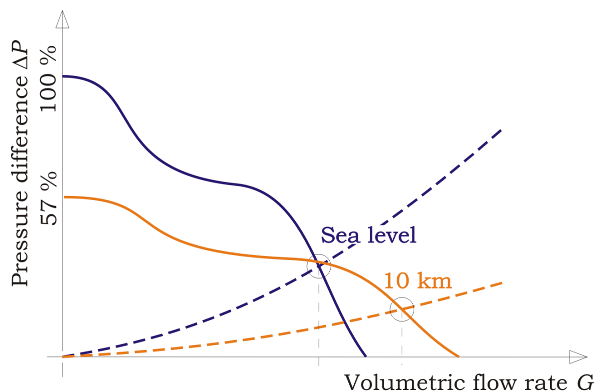

(b) Altitude compensating fan and turbulent flow.

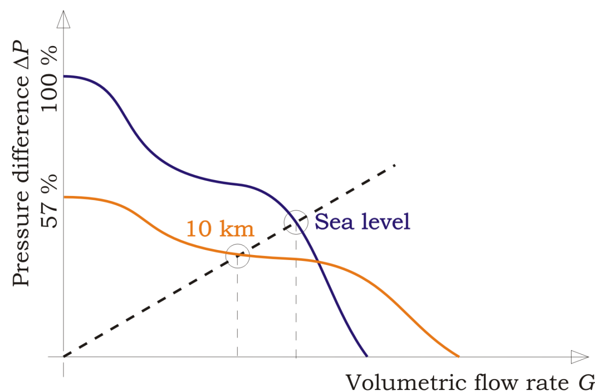

(c) Altitude compensating fan and laminar flow. The system resistance curve is independent of altitude for laminar flow.

Figure 6.2: Dependence of operating point for the two different fan types. For this example, the altitude compensating fan is assumed to run at a 30 % increased speed at an altitude of 10 km. System resistance curves are depicted in dashed lines.

There are two different kinds of fans: *constant speed fans* (also called *conventional fans*) and *altitude compensating fans* (also called *slip fans*). Conventional fans always run at the same speed, which results in constant volumetric flow rates according to Eq. (6.10). Slip fans partly compensate the decreased density and therefore reduced cooling effectiveness at higher altitudes by increasing their speed due to the decreased load on the fan.

While dimensioning the cooling system with a conventional fan for the worst case at high altitudes is possible, the cooling system would have excess performance at sea levels. This shows in unnecessarily high power consumptions. Depending on the fan, the fan motor's waste heat is often dissipated by the same fluid flow. Hence, higher power consumptions lead to higher fluid inlet temperatures. Further disadvantages of a conventional fan at lower altitude are increased noise and, more important, mechanical stresses and wear, which lead to a shorter lifetime. An altitude compensating fan, on the other hand, provides a higher volume flow rate just for lower densities.

Figure 6.2 shows the dependance of the operating point on altitude. As an example scenario for a conventional fan (Fig. 6.2(a)), the density ratio ρ_a/ρ_0 is about 0.34 for an altitude of 10 km according to the International Standard Atmosphere [3]. This is exactly the ratio by which the pressure difference Δp and the system resistance for turbulent flow will be decreased, according to Eq. (6.11) and (6.8), respectively. Therefore, volumetric flow rate does not depend on altitude for turbulent flow. It has to be noted

that the mass flow rate, which is the relevant factor for the cooling effectiveness, is decreased to the same 34 % according to Eq. (6.6).

An altitude compensating fan behaves differently. The fan speed increases with altitude, which is assumed to be 30 % at an altitude of 10 km for this example. The volumetric flow rate increases by the same amount, according to Eq. (6.10). The pressure drop is both affected by speed and density. It decreases by 43 % according to Eq. (6.11). This defines the fan performance curves at 10 km in Fig. 6.2(b) and 6.2(c).

The system resistance curve depends on density and therefore altitude just for turbulent flow. The resulting operating points are highlighted in Fig. 6.2(b). The volumetric flow rate increased with altitude, which is an improvement in comparison to the constant speed fan.

For laminar flow, the linear system resistance curve does not depend on density as shown in Fig. 6.2(c). Despite the altitude compensating fan, the volumetric flow decreases for higher altitudes (as opposed to the constant flow rate for a conventional fan and turbulent flow). This is the reason why a turbulent flow heat sink should be considered for unpressurized locations in aircrafts.

Closed-loop controls. An altitude compensating fan runs at different speeds for different altitudes, but it does not necessarily completely compensate for the lower density at higher altitudes, depending on system design and fan specifications. An alternative is a conventional fan whose speed is controlled by a closed loop system. Although the overall system still has to be designed for the worst case, the fan does not have to operate at its maximum for many scenarios.

The feedback circuit is based on one or several sensor outputs, which typically measures the temperature at critical spots in the design. This information can also be used in order to monitor system performance and to set off an alarm in case of a failure. A simpler fan-speed sensor could not detect failures in the flow pass, e. g. blocked filters.

The disadvantage of this approach are the increased complexity as another electric circuit is needed. As for any closed loop system, it has to be ensured that the system does not oscillate. This should not pose a major challenge due to the rather slow responses of thermal systems.

Influence of altitude on heat transfer coefficient and therefore ΔT_B. The heat transfer coefficient h is directly proportional to the Nusselt number, see Eq. (4.17). The Nusselt number for fully-developed turbulent flow in circular pipes is given in Eq. (4.22). Taking Eq. (4.14) and (4.15) into account and combining constants to C, the heat transfer coefficient as a function of density (and therefore altitude) and volumetric flow rate is

$$h = C\rho^{0.8}G^{0.8} \,. \tag{6.13}$$

It follows that

$$\Delta T_B \sim \frac{1}{\rho^{0.8}G^{0.8}} \,. \tag{6.14}$$

For constant speed fans, the volumetric flow rate does not depend on altitude.

Hot spot surface temperature T_S depending on altitude. Cooling effectiveness decreases with increasing altitude due to a lower air density at higher elevations. This effect is somewhat compensated by a reduced ambient temperature at higher altitudes.

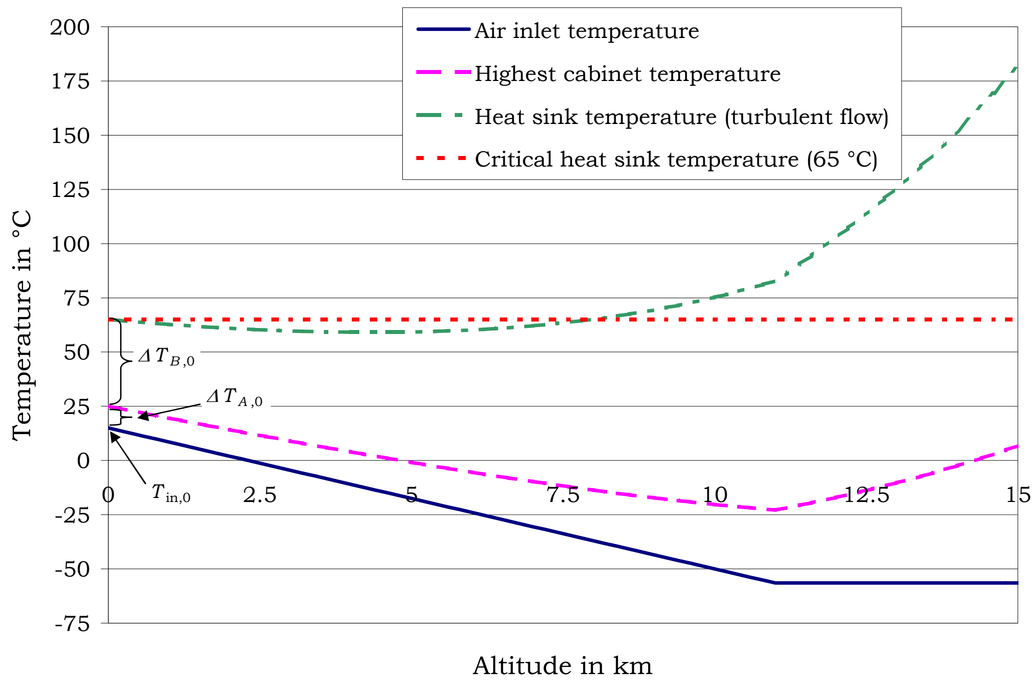

(a) $T_{\text{in},0} = 15$ °C, $\Delta T_{A,0} = 10$ K, $\Delta T_{B,0} = 40$ K. Heat sink temperature is already exceeding requirements at about an altitude of 8 km.

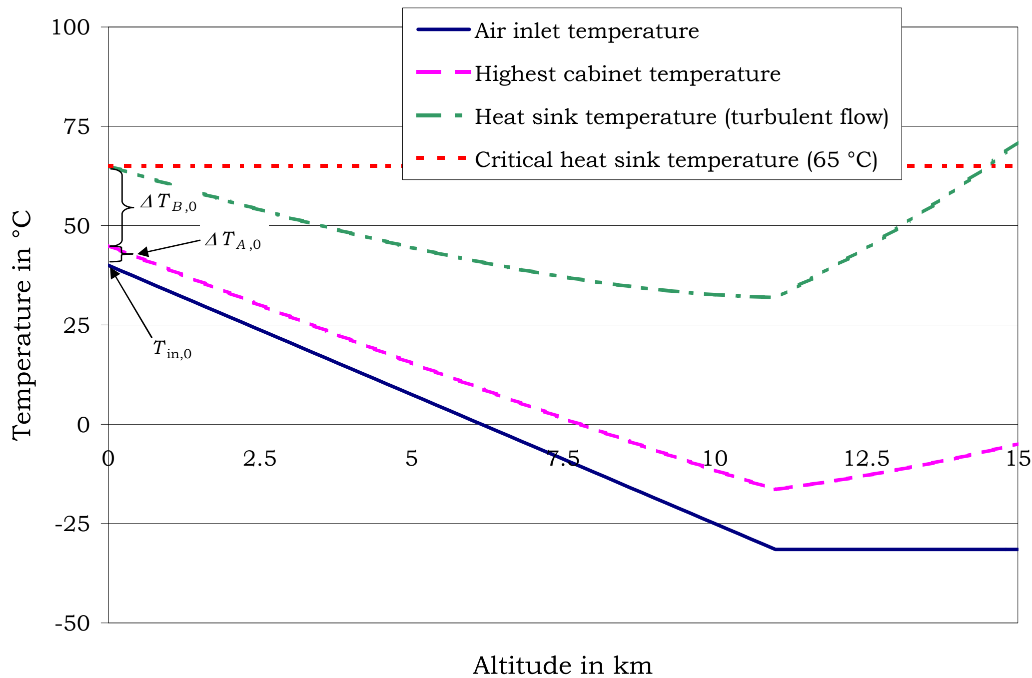

(b) $T_{\text{in},0} = 40$ °C, $\Delta T_{A,0} = 5$ K, $\Delta T_{B,0} = 20$ K. Heat sink temperature does not exceed temperature requirements for altitudes below 14 km.

Figure 6.3: Exemplary dependence of heat sink temperature from altitude for the turbulent flow case utilizing a constant speed fan. Two different sets of inlet temperatures T_{in} and temperature differences $\Delta T_{A,0}$ and $\Delta T_{B,0}$ at sea-level are assumed.

In order to find out if the maximal heat sink temperature of 65 °C (see Sec. 3.3) is exceeded for higher altitudes, the temperature differences $\Delta T_{A,0}$ and $\Delta T_{B,0}$ at sea-level have to be known.

Figure 6.3 shows an exemplary correlation for an non-pressurized area. Since ΔT_A depends on the volumetric flow rate and, simply spoken, therefore on the size of the fan, the figure is chosen to be small. Generally, a larger fan is always an option. ΔT_B, on the other hand, depends on the heat sink geometry, which is constricted by assembly constraints (no direct contact of air with electronics, maximum thickness of 5 mm). Hence, the number was chosen to be large as opposed to ΔT_A. As discussed before, the inlet air cannot be directly taken from the outside. The preconditioned air is assumed to have a temperature of 15 °C and 40 °C at sea-levels for Fig. 6.3(a) and 6.3(b), respectively. It is assumed that the preconditioning system maintains a fixed temperature difference between the outside air inlet and the air which is supplied to the fan inlet.

Figure 6.3(a) shows that the heat sink temperature exceeds the requirements for an altitude above 8 km. The decreasing outside temperature does not compensate the decreasing air density as is the case for the second example depicted in Fig. 6.3(b). It can be concluded that the influence of altitude can be both positive and negative, depending on the specific system design.

6.2.2 Possible designs and simulations

Heat sinks are usually build out of a material with high thermal conductivity like copper or aluminum. They are based on the principle that an increased contact surface for the fluid increases cooling effectiveness. This is not true by itself as flow resistance and fin efficiency influence the overall performance as well.

Commercially built fin heat sinks belong most often to one of the following categories:

- *Extruded heat sinks* are made out of a single piece of metal. They are usually low-priced, made out of aluminum, and the most common choice for a variety of applications.
- The fins of a *folded fin heat sink* are made out of a single sheet of material in a wavelike manner bonded (solder, braze, or epoxy) to one or two solid plates which act as a heat spreader and/or direct the fluid flow. The main advantage are thin fins and the possibility to combine two materials for fins and baseplates. Thin fins are beneficial for thin heat sinks since they allow for a better air flow and reduced weight. For thicker heat sinks, the reduced fin efficiency of thin fins becomes a disadvantage.
- *Bonded heat sink* are very similar to folded heat sinks. The difference is that the fins are made out of several plates which are separately bonded to the base plate. The critical point of the design is the quality of the joint since it can greatly increase the thermal resistance.
- *Die cast heat sinks*, which are mostly made out of aluminum (although copper is another possible material), can be mass-produced in more complex shapes than it is possible for the other methods mentioned before. The fins cannot be produced as thin as for folded fin heat sinks, for example.
- To overcome the disadvantage of die cast heat sinks, *cold forged heat sinks* were developed. Thin and high fins can be fabricated.

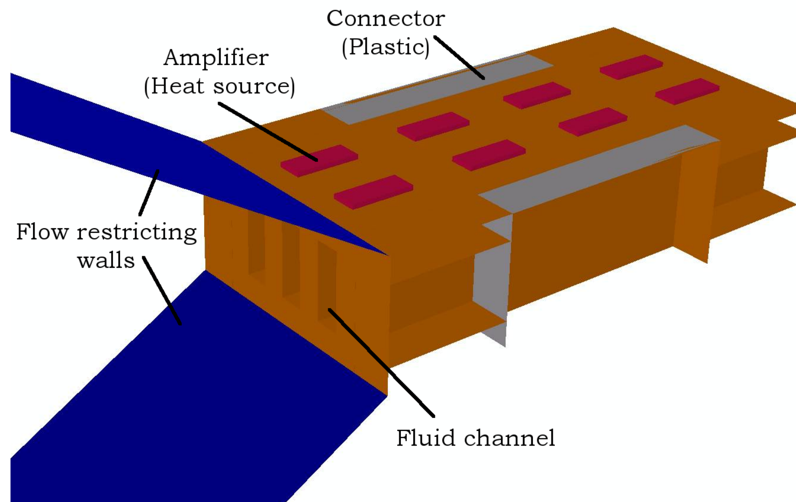

Figure 6.4: Design 1. The three fluid channels are 1 mm wide and 3 mm high. The copper cold plate is 20 mm long.

- *Milled heat sinks* are usually expensive, but special geometries made out of a variety of materials can be realized.

The fins can be shaped and arranged in many different ways. Often used forms include *plate fins* and *pin fins* with square or circular cross-sections arranged *in-line* or *staggered*. The surface is often treated. A black surface increases thermal radiation, which can especially improve cooling efficiency for natural convection heat sinks. For forced convection heat sinks, this improvement is secondary.

Design 1: Based on liquid cold plate

The first design was numerically simulated in order to verify the basic principles in forced air convection and to get an insight about the accuracy of Flotherm. The utilized geometry is the same as the one described in more detail in Sec. 6.3.2 for liquid cooling. The practical thought behind this approach was that the liquid cold plate could be utilized in a forced air cooling system for a smaller demonstration model (like 4×4 elements instead of 50×50 elements) and thereby abandoning the need to install a more complex liquid cooling system.

The ambient air was set to a temperature of 20 °C at sea-level. Many antenna elements will be placed next to each other in the final design. Due to the repetitive pattern of the overall antenna array, only a small stripe (2 elements wide) is necessary for the numerical model to assess the overall performance while neglecting side effects and assigning symmetry boundaries at the appropriate walls of the computational domain (see Fig. 6.4). Flow restricting walls had to be added to the numerical model in order to force the air flow through the channels.

Allowing for a maximum temperature difference between inlet and outlet of 10 K, the volumetric flow rate of the fan was set to $2.83 \cdot 10^{-3}$ m^3/s (6 cfm).

In a first run, the volumetric flow rate was set to be constant, neglecting the fan curve and assuming that the fan could provide any amount of pressure difference. The resulting outflow temperature agreed within 1 K with the expected temperature difference; the heat sink hot spot temperature was 34 °C. Although these results sound promising,

the pressure difference required to force the flow through the channels has to be considered as it is substantial. The pressure drop was 60 kPa (0.6 bar), resulting in a flow speed of 275 m/s inside the channels. This value is beyond any practical application. As a comparison, an exemplary commercial fan with a size of $120 \times 112 \times 30$ mm^3 is able to provide a maximum pressure difference of 470 Pa [38].

The fan curve of the previously mentioned commercial fan was taken into account in a second run, which lead to realistic pressure drops across the air inlets and outlets of the cold plate. Now the fluid velocity inside the channels is 26 m/s and the outflow temperature rises to 100 °C. The heat sink hot spot temperature is 205 °C and therefore far exceeding the cooling requirements for the amplifier.

Design 2: Ideal fin spacing

The previous design was easy to fabricate due to the rather thick fins and fluid channels. Anyway, from the thermal point of view, the design was not ideal. For the second design, the thermal characteristics were improved to answer the question if a forced convection air cooling for the given thermal problem is possible at all.

The geometry was simplified in order to improve the cooling effectiveness. The connectors were removed and it was assumed that no holes for connectors were necessary, leading to an increased width for possible fluid channels. The requirements of a maximum cold plate height of 5 mm and no direct air contact with electronics were maintained. The fin width was chosen to be as small as possible. Commercially available folded fin heat sinks use fin widths down to 0.2 mm, and this value was taken. Otherwise, the overall design was identical with the one shown in Fig. 6.4, where 8 amplifier dissipating 3.8 W each (totalling to 30.4 W) were included. The inlet temperature was once again set to 20 °C. It was assumed that the heat sink was fabricated out of one piece, and therefore thermal resistances which would otherwise occur due to bonding the fins to the base plates were neglected. The approximated fin curve of the previously mentioned blower [38] was included in the simulation. The fan's dissipated power (19.7 W, which would add 65 % to the overall dissipated power) was not included at this stage.

Increasing the number of fins increases the area exposed to the fluid flow, but it also increases the flow resistance. An ideal fin spacing exists, and it was found numerically using Flotherm to be 0.51 mm for this geometry and blower. The maximum temperature was 115 °C, exceeding the requirements even for this simplified case of only 4 amplifiers along the direction of the fluid channels (instead of up to 50 for the complete antenna array). A cross-sectional view of the geometry showing the temperature distribution can be seen in Fig. 6.5. The temperature along the fins is practically constant (the fin efficiency is close to 1), which justifies choosing thin fins.

Further analysis on the model with ideal fin spacing confirmed the assumption that the hot spot temperature is a linear function of input power. The hot spot temperature, for the case of only four amplifiers along the direction of the fluid flow, decreased to 65 °C for an input power of 1.8 W per amplifier (instead of 3.8 W). Extrapolating this result to an array with 50×50 elements would allow a maximum dissipated power of 144 mW per amplifier. Once again, this result is just valid for the simplified model, i. e. no wholes for connectors are included in the cold plate, which would decrease the available space for fluid channels and diminish the cooling effectiveness.

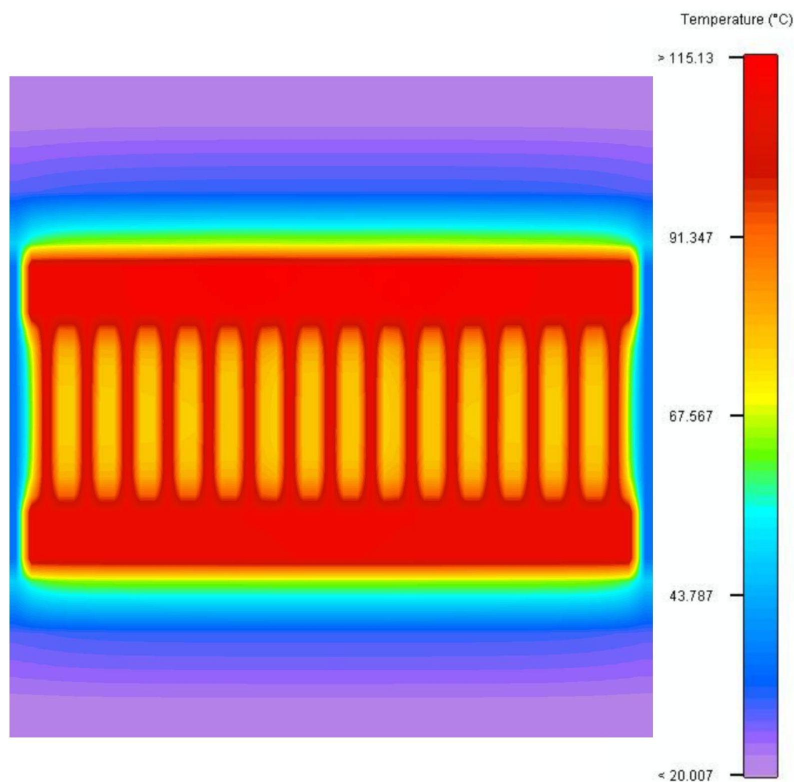

Figure 6.5: Design 2 with ideal fin spacing for 3 mm high fins. The maximum heat sink temperature is 115 °C.

Conclusion. It has to be concluded that the array cannot be sufficiently cooled by forced air convection despite simplified assumptions and while limiting the fin heat sink thickness to 5 mm. A necessary fan or blower would be exceedingly large and heavy compared to the antenna array, and the air mover's dissipated power would considerably add to the overall heat flow.

Design 3: Model with 4 × 4 elements

The third design is not thought to cool down the complete antenna array with 50 × 50 radiating elements. It was rather designed to be used for a demonstration model consisting of 4 × 4 elements (totalling to 60.8 W of dissipated power). A forced air cooling was chosen since it can be installed with greater ease than a liquid cooled system. The characteristics of the used fans and fin heat sinks were selected so that comparable parts are easily commercially available. Since the demonstration model will have to prove the whole concept, the cold plate thickness and the design for connectors were not modified. The ambient conditions were set to an air temperature of 20 °C at sea level.

The design is shown in Fig. 6.6. It was ensured that no parts are extending above the plane in which the amplifiers are mounted. The radiating elements are located very closely to the amplifiers so that metal parts extending into the antenna's beam direction might influence the antenna performance. Furthermore, the fins are aligned that way that warm air is not being blown in the direction of the electronics, which are located below the amplifiers and are not shown in Fig. 6.6. The geometry can be summarized as follows:

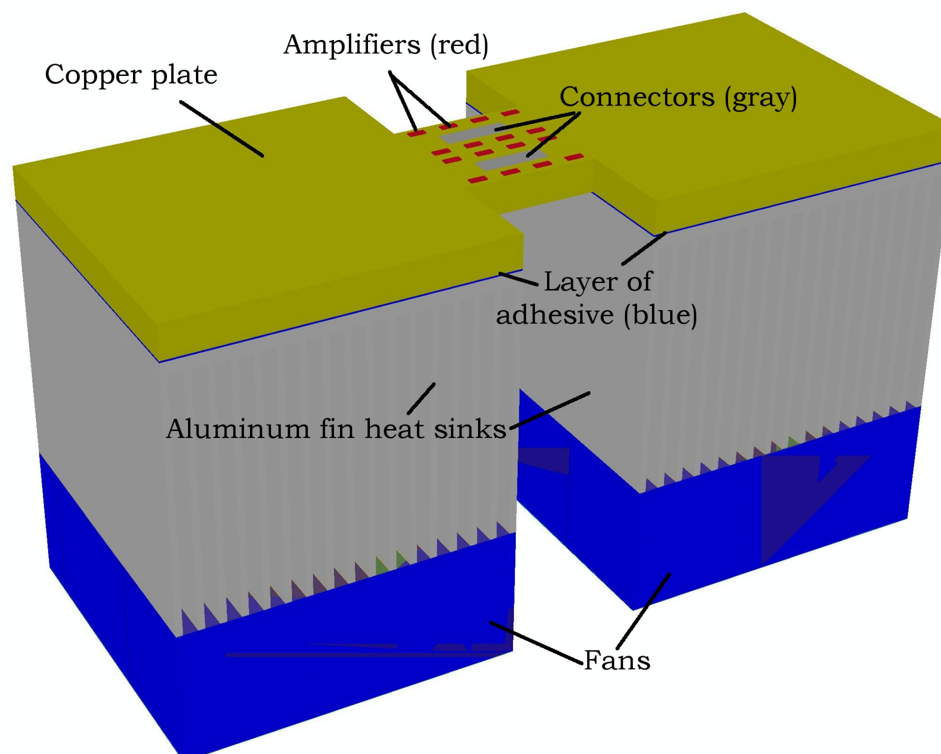

Figure 6.6: Design 3 for 4 × 4 elements. The fans have a side length of 50 mm each, the heat sink is 40 mm high.

Cold plate: The copper cold plate is 5 mm thick, 50 mm wide and 120 mm long. The square part in the middle, on which the amplifiers are mounted, has a side length of 20 mm. The amplifiers and cut outs are positioned as shown in Fig. 3.3.

Extruded fin heat sink: The heat sinks are made out of aluminum and are 40 mm high. The fins are 38 mm long and 1 mm thick. The spacing between the fins equals 2 mm.

Fan: The fan's outer diameter is 50 mm, the hub diameter is 22 mm.[2] The fans run at 5000 rounds per minute in a counter-clockwise direction as seen from above. They blow the air towards the heat sink and dissipate 2.52 W each (which was included in the numerical simulation). The linearized version of the fan curve with a free flow rate of $7.32 \cdot 10^{-3}$ m^3/s and a pressure drop at stagnation of 18.9 Pa was taken into account.

Adhesive: The adhesive layer was assumed to be 0.25 mm thick. The thermal conductivity was set to 1.05 W/(m K).[3]

The temperature distributions for two cross-sectional views are shown in Fig. 6.7. The geometries symmetry was exploited for the simulations to decrease computational time. This is why temperature distributions are not shown for the whole design. The

[2]The fan's characteristics are based on the model F-520H12 S/C/B2 [39], which is available from CofanUSA. Similar fans should lead to similar results.

[3]This data was based on the commercially available adhesive Elecolit® 6601 [40], distributed by Panacol-Elosol. The company could not provide data with respect to deterioration of thermal conductivity over time.

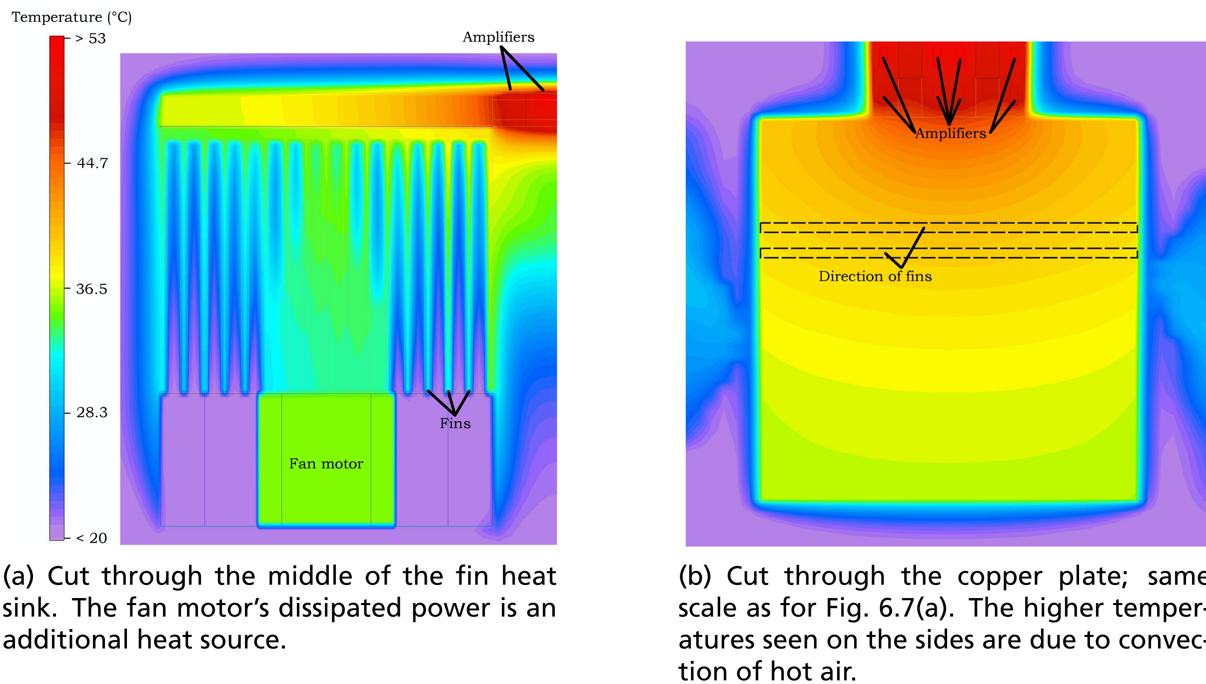

(a) Cut through the middle of the fin heat sink. The fan motor's dissipated power is an additional heat source.

(b) Cut through the copper plate; same scale as for Fig. 6.7(a). The higher temperatures seen on the sides are due to convection of hot air.

Figure 6.7: Cross sectional views of design 3 showing temperature distributions.

warm air being blown away from the fin heat sink, as can be seen in Fig. 6.7(b), is not distributed symmetrically for the left-hand and right-hand side. This is due to the swirl of the fan (running counter-clockwise as seen from above).

The most interesting figure in assessing the quality of the design is the maximal copper-plate temperature on which the amplifiers are mounted. The simulations showed that the maximal temperature is 55 °C, which leaves a difference of 10 K to the allowable maximum of 65 °C. This shows that a forced air cooling for a 4×4 array based on standard components is possible, and no specific optimizations (especially shaped fins or especially powerful fans, for instance) are necessary.

Material inferface. The contact between the fin heat sink and the copper plate (here realized by an adhesive) adds to the thermal resistance. The partially insulating effect can be seen in Fig. 6.7(a). Setting the material properties of the adhesive equal to the ones of the heat sink (ideal case), the maximum copper-plate temperature decreases to 51 °C. While other mounting techniques than adhesive bonding are possible (e. g. screw joint), a good contact has to be ensured. Due to the nearly inevitable roughness of the surfaces involved, the joint usually only consists of many contact spots while voids filled with air form in between [41]. Thermal interface materials like grease can greatly diminish the thermal resistance of joints by filling up the voids.

6.3 Forced liquid cooling – Cold plates

A cold plate is similar to a fin heat sink as it transfers heat from a surface to a fluid. The fluid being a liquid here is forced through the cold plate by means of a pump. The heat, which is now stored in the fluid, has to be dissipated somewhere else. A heat exchanger can transfer the heat to another liquid, or to the ambient air. A closed-loop liquid cooling system, as seen schematically in Fig. 6.8, is completed by a storage and

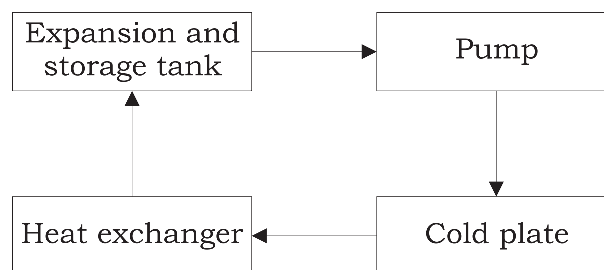

Figure 6.8: Basic liquid cooling system.

expansion tank. Its purpose is to protect the system from increasing pressures due to the expansion of the heated fluid, and to supply sufficient amounts of fluid to the loop at all times.

The general similarity to fin heat sinks is also expressed in the same equations, which were presented in Sec. 6.2. The basic improvement upon forced air cooling is the increased specific heat and thermal conductivity of liquid coolants as opposed to air. The fluid flow rate and system size can be considerably reduced. Often, a liquid cooled system is less heavy and smaller than a comparable forced air cooling system despite the added weight of pipes and coolant.

The main disadvantage of a liquid cooling system is the increased system complexity. Building a system which is sealed in all situations is more complicated (and expensive) than a forced air cooling system. Once fluid leaks out of the system, electronics can be electrically (shorts), chemically (aggressive fluids), and thermally (hot fluid) destroyed. In the context of avionics, more effort is necessary to comply with security specifications. This is certainly one reason why most avionics cooling systems are forced air cooling systems.

Another disadvantage of a liquid cold plate is that the array cannot be build modular without changing assembly constraints as indicated in Sec. 3.1. By modular, an array out of several sub-assemblies with, for instance, 4×4 elements is thought of. This is due to the fact that no feeding pipes can be mounted on the reverse side of the array because of space considerations, and a sealed system would be very difficult to obtain for channels going through different sub-assemblies. A modular approach would allow to individually fabricate and test sub-assemblies. In case of failure during later operation, not the whole array needed to be replaced. A modular approach would become possible by deviating from the assembly constraints. If components on the reverse side of the array could be arranged in a manner which allowed tube fittings, a modular approach might become possible.

A pump has to overcome flow resistance much the same way as fans have to work against the system resistance. The lower the flow resistance, the less pressure the pump has to supply. This results in a smaller pump and therefore less dissipated pump power (which adds to the overall heat load). The causes for pressure drops in a liquid cooled system are:

- friction (depending on surface roughness and liquid velocity),
- elevation (if the liquid has to be pumped against gravity), and
- losses due to liquid guiding (elbows, transitions, etc.).

The third factor dominates for most systems. Pressure losses due to typical bends and transitions are known; the same is true for various pipe entrances, where a rounded off entry results in less pressure drop than a square edge entry, for instance [26].

Since an array size of 50 $\times$ 50 elements seems to be most likely at this stage of the project, the development of a cold plate will be focused on this array size. Due to the repetitive structure of the array, similar results could be easily yielded in an analogous manner for larger or smaller arrays.

6.3.1 Design considerations

Keeping in mind that the cold plate thickness is not to exceed 5 mm (see Sec. 3.1), it becomes apparent that liquid channels have to be oriented in parallel to the layer containing the patches as shown in Fig. 3.2 on page 6.

The thermal resistance of the cold plate can be decreased by decreasing ΔT_A and ΔT_B according to Eq. (6.4). Equation (6.5) indicates that ΔT_A can be reduced by increasing the mass flow rate $\dot{m}$ and by choosing a liquid with a high specific heat c. This summand is correlated to the cold plate design by the flow resistance since a higher flow resistance yields a lower mass flow rate for a given pump.

The second summand, ΔT_B, is described by Eq. (4.11). Therefore, the surface A and the heat transfer coefficient h should be as large as possible. The surface can be increased by increasing the number of channels. This results in thinner channel walls and smaller channel cross-sectional areas since the overall width of the array cannot be modified. This approach is limited by two factors: the wall width (since thin walls are more complicated to manufacture and are less mechanically stable), and the increased flow resistance (influencing ΔT_A).

It is advantageous to build the cold plate out of one block of material since every material interface introduces another additional thermal resistance. Analogous to a folded fin heat sinks for forced air cooling, the channels of the cold plate could be build out of a folded thin layer of material. This would simplify machining as opposed to milling such a heat sink. The flow would be restricted by two cover plates, which are bonded to the channel structure.

The second factor determining ΔT_B, the heat transfer coefficient h, is described by the Nusselt number. Higher Nusselt numbers yield better heat transfer. As described in Sec. 4.2.3, turbulent flow is therefore desired. Turbulent flow is more likely to occur for larger channel diameters, higher fluid velocities, and lower kinematic viscosities (see Sec. 4.2.1). Assuming turbulent flow and combining Eqs. (4.3), (4.14), (4.17), (4.18), and (4.22), one yields the following function for the heat transfer coefficient:

$$h = 0.0235 \cdot \frac{\lambda^{0.52}(\rho c)^{0.48}}{\nu^{0.32}} \cdot \frac{v^{0.8}}{d^{0.2}} \, . \tag{6.15}$$

Therefore, the heat transfer coefficient increases for increasing

- thermal conductivity (fluid),
- density (fluid)
- specific heat (fluid),
- fluid flow velocity,

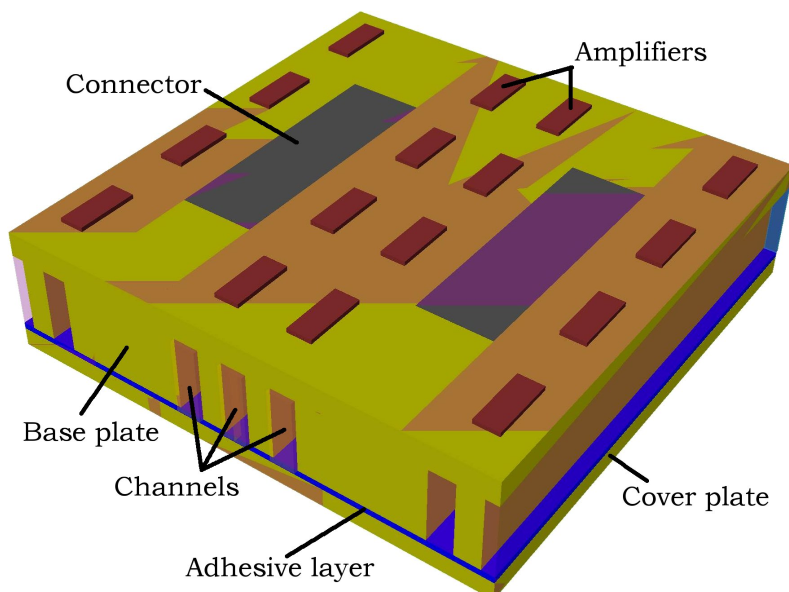

Figure 6.9: Cold plate section. Due to geometry symmetries, only the volume between the midplanes of the connectors needed to be in the computational domain.

and decreases for increasing

- kinematic viscosity, and
- channel diameter.

To give a numerical example, an array with 50 $\times$ 50 elements is considered. The worst case dissipated power is 9.5 kW. If the working fluid is water and a fluid temperature rise ΔT_A of 10 K is allowed, the volumetric flow rate would have to be 227 ml/s (or 3.6 gallons per minute) according to Eq. (6.5). A maximal fluid temperature difference of 10 K between inlet and outlet ensures a sufficiently small temperature gradient across the array, which simplifies calibration.

If the water inlet temperature is supposed to be 25 °C, ΔT_B should be below 30 K so that the hot spot temperature does not exceed 65 °C according to Eq. (6.4). Therefore, the thermal resistance (as given in Eq. (4.7)) of the cold plate is not to exceed 3.16 mK/W.

6.3.2 Design for 50 $\times$ 50 elements

A section of the cold plate design for an array with 50 $\times$ 50 elements is shown in Fig. 6.9. It resembles a sub-assembly of 4 $\times$ 4 elements. The cold plate is made out of copper. The base plate, on which the amplifiers are mounted, has a hight of 4 mm. The channels have a cross-sectional area of 1 $\times$ 3 mm^2. The channel walls are 1 mm thick. The flat copper cover plate is 1 mm thick. It is bonded to the base plate by a thermally conductive adhesive (Elecolit 6601 [40]).

The advantages of this design are that there are liquid channels directly below every amplifier, which ensures a good thermal coupling. Previous designs with just one channel per sub-assembly of 4 $\times$ 4 elements showed that heat was ‘trapped’ behind the connectors due to the limited thermal conductivity of the copper base plate. Three channels were incorporated below every row of two amplifiers. This is advantageous

Material	Specific heat kJ/(kg K)	Dynamic viscosity 10^{-3} kg/(m s)	Temperature range °C
Coolanol 25 @ 25 °C	1.884	4.5	−60 to 300
PAO @ 38 °C	2.26	42.3	−48 to 130
Water @ 25 °C	4.178	0.896	0 to 100

Table 6.1: Properties of some coolants [26, 42].

since the available surface area is increased as opposed to a design with only one wide channel. Since the liquid flows in a straight line, no pressure losses due to bends are being encountered. The arrangement of connectors and amplifiers, as shown in Fig. 3.3, works very well since the connectors pose no obstacle for the guiding of the liquid channels. Furthermore, the amplifiers are arranged in a repetitive manner so that only one feeding network design is sufficient for all elements.

The design with 1 mm wide channels and 1 mm wide channel walls is rather massive. Although the design could be optimized with respect to height and thermal performance, this would come at a cost of a more complicated construction. Since the simulation results were to be confirmed by experiments, an actual cold plate had to be build in reasonable time and by means of available tools, which results in a strong argument for the current design.

Fluid inlets and outlets can easily be attached at the sides of the cold plate (for an example, see Ch. 7). The fluid flow does not necessarily have to be supplied by only one pump. Several smaller pumps can be connected to a subset of the channels. This would allow a modular approach so that stripes (along the fluid channels) of the antenna could be build and tested independently. The increased thermal resistance at the interfaces is acceptable since no heat flux is directed across the interface.

By incorporating several pumps in the cooling loop, one can introduce redundancy. This might be important for security relevant applications so that failure of one pump alone does not cause a total breakdown of the cooling system.

6.3.3 Coolants

Choosing the right coolant for a liquid cooling system depends on the following factors:

- operating and storage temperatures and pressures,
- specific heat,
- viscosity,
- density,
- compatibility with all wetted system materials, and
- handling considerations (flammability, environmental impact).

Some common liquid cooling fluids are listed in table 6.1. The disadvantage of water is the limited usable temperature range, which is increased for other coolants. The main advantage of water is its high specific heat, which allows lower flow rates than for

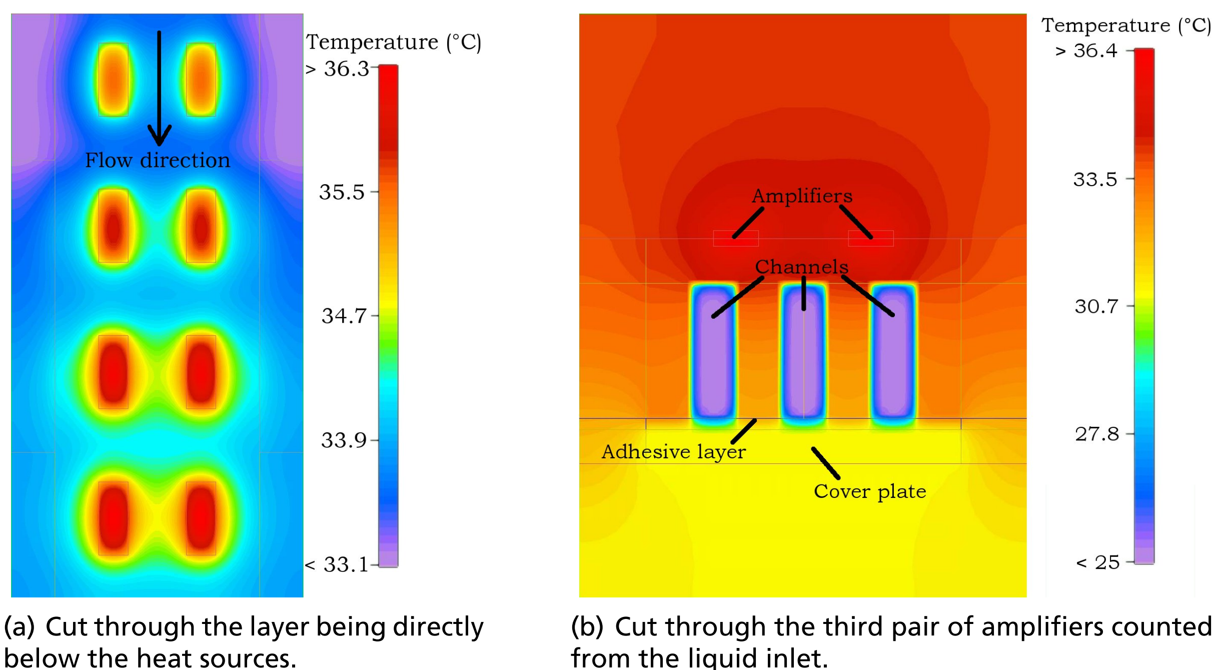

(a) Cut through the layer being directly below the heat sources.

(b) Cut through the third pair of amplifiers counted from the liquid inlet.

Figure 6.10: Computational results for geometry as shown in Fig. 6.9.

other typical coolants. Since the water temperature range is sufficient for cooling the antenna array, and since the combination water and copper (as the cold plate material) works very well, water is selected as the coolant.

6.3.4 Simulation

Simulation of an array with 50 $\times$ 50 elements would take up immense computer and time resources. Fortunately, the structure of the array is repetitive so that applying adequate symmetrical boundary conditions allow to examine only a sub-assembly (stripe of 2 $\times$ 4 amplifiers) as shown in Fig. 6.9. This neglects effects at the sides, but since temperatures at the sides of the array are expected to be lower than in the center, the current approach resembles the worst case.

Temperature distributions for this sub-assembly are shown in Fig. 6.10. Each amplifier was assumed to dissipate 3.8 W (worst case), and the water inlet temperature was set to 25 °C. The volumetric flow rate per channel was given as 3 ml/s, which is the proportional fraction of the before stated 227 ml/s for the whole array.

The hot spot temperatures directly below the heat sources in Fig. 6.10(a) range from 35.6 °C for the first row of amplifiers to 36.4 °C for the last row of amplifiers. The difference of 0.8 K represents very well the water temperature rise of 0.8 K according to Eq. (6.5). Indeed, a simulation with a stripe of 2 $\times$ 52 elements revealed a hot spot temperature difference between the first and last row of amplifiers of 10.5 K, which is very close to the expected 10.4 K. Therefore, the temperature difference across the array is governed by the temperature rise of the water, which can very well be predicted by Eq. (6.5). If a temperature difference of less than 10 K should be become necessary later on, the required flow rate could thus easily be determined.

The results for the stripe of 50 $\times$ 50 elements for the stated flow rate suggest a maximal water inlet temperature of 43 °C to enforce a hot spot temperature which does not exceed 65 °C. Lower temperatures can be obtained by raising the fluid flow rate.

To conclude, the presented cold plate meeting the dimension constraints is very well able to cool down the antenna array. A total water flow rate of 227 ml/s at an inlet water temperature of about 25 °C for a 50 × 50 element array ensures a maximal temperature difference of 10 K across the array while keeping the hot spot temperature far below 65 °C.

6.3.5 Perspective

Improvements with respect to size and weight are possible, but they come at a cost of a more complex design. A commercially available copper cold plate from Lytron, type CP40 [43], features a plate thickness of 2.5 mm. Cut outs (for mounting components) are incorporated in the design, showing that they are generally possible. The cold plate contains crossed micro-channels. The advantage is turbulent liquid flow (better heat transfer), but on the other hand, a resulting higher pressure drop requires a more powerful pump.

6.4 Peltier coolers

A Peltier element (also called a thermoelectric converter or TEC) is a heat pump based on the Peltier effect. By applying an electric current, one side heats up while the other cools down. Its main advantage is to be able to cool down a surface below ambient temperature. As a cooling device, the cold side is attached to the heat source while the warm side is connected to a heat sink (which is often a forced convection fin heat sink, but other heat sinks are possible as well). It's main disadvantage is that the electric current adds to the total heat load so that the heat sink has to dissipate more power than without a Peltier module. Depending on the specific characteristics of a design, a heat sink coupled to a Peltier element can therefore result in higher component temperatures than the heat sink by itself.

Geometrically, Peltier modules are flat plates where the two large surfaces heat up or cool down, respectively. If the cold plate in Fig. 3.2 were replaced by a Peltier element, the heat sink would have to be mounted where the circuit boards are placed. This renders the elements unfit to cool down the antenna array since heat has to be removed to the sides.

6.5 Heat pipes

A heat pipe is able to transfer large amounts of heat in a two-phase flow system noiseless with no outside power at a very low temperature difference. A typical heat pipe consists of a hollow, sealed metallic cylinder whose inner walls are covered with a capillary structure (called wick) as shown in Fig. 6.11. The tube is partly filled with a working fluid. If the one end is heated up, the liquid evaporates and the vapor drifts due to the pressure difference to the cold end. This condenser zone is connected to a heat sink by means of thermal conduction. The vapor condenses at the walls and travels back completing the circle to the heat source through the wick by means of capillary action.

Five limits exist which restrict the performance (power rating) of a heat pipe:

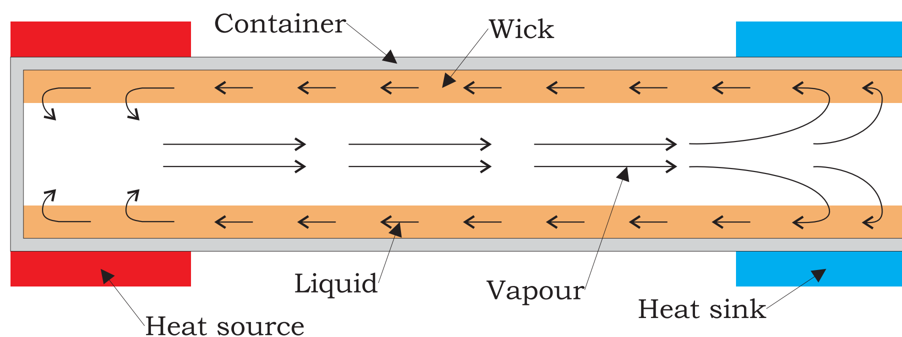

Figure 6.11: Cross-sectional view of a heat-pipe with condenser and evaporator region.

Viscous limit: The viscosity of the vapor flow limits the heat flux for low temperatures, which occur during the start-up phase.

Sonic limit: The velocity at which vapor can travel from the evaporator to the condenser is limited.

Entrainment limit: The liquid and vapor flow are contradictory. At the interface, the vapor flow can cause liquid droplets to be entrained into the vapor flow. This can finally result in a heat pipe dry out.

Capillary limit: If the pressure drop between the evaporator and condenser zone exceeds the contrary capillary pumping pressure, the heat pipe stops to operate. The pressure is inversely proportional to the effective radius of the interface.

Boiling limit: High heat flux at the evaporator results in boiling of the fluid. The vapor bubbles result in a cut off of the capillary action so that the evaporator zone dries out.

The operation of the heat pipe is further restricted to the temperature zone ranging from the fluid's freezing point to it's critical point. Usually, the limiting factor is the restricted capillary force available, which depends on the wick. Choosing the right wick structure is a compromise between a low liquid flow resistance and a high capillary pumping pressure. A low flow resistance is required for high heat loads while high pumping pressures are needed for heat pipes operating against gravity (i. e. the condenser is below the evaporator). The two extremes in terms of pumping pressure and permeability in wick structure design are

- groove wicks, which are simply made out of axial grooves in the supporting tube, and
- sintered powder metal wicks.

It was shown that metal powder wicks are far less affected by vertical alignment as groove wicks [44]. Many other wick structures exist to fulfill different needs [45]. Generally, heat pipes work best in a vertical position where the evaporator is below the condenser. Horizontal orientation is generally well supported. For vertical orientation where the condenser is located below the evaporator, special heat pipes supporting large capillary action are required or the nominal power rating decreases considerably.

In the avionics environment, other forces than gravity have to be considered. Investigations on a special water filled flat copper mesh heat pipe under unfavourable accelerations were conducted [46]. The especially built heat pipe was 150 mm long, 50 mm

Medium	Temperature in °C	
	Minimum	Maximum
Ammonia	−60	100
Acetone	0	120
Methanol	10	130
Flutec™ PP2	10	160
Ethanol	0	130
Water	30	200
Toluene	50	200

Table 6.2: Possible working fluids for heat pipes, from [47].

wide, 2.4 mm thick, and was designed for a nominal power of 60 W. It showed that transient accelerations up to 10 g increased the thermal resistance not more than 70 % for all orientations.

The used working fluid influences the temperature range and performance of the heat pipe. The performance depends on the surface tension of the fluid, which is important for the capillary force, and the latent heat as the performance is directly proportional to it. The working fluid also limits the materials which can be used for the wick and the container since the working fluid has to be chemically compatible with all used materials to avoid corrosion. Possible working fluids and according temperature ranges are listed in Tab. 6.2. In general, heat pipes exist for a temperature range from −263 °C up to about 5000 °C [48]. A typical material and working fluid combination is water and copper. This is partly due to the high latent heat of water.

6.5.1 Micro heat pipes

Miniaturization of heat pipes led to designs which work without a capillary structure. The wick is replaced by small arteries (with diameters down to 20 μm [49]) featuring sharply cornered cross-sections like triangles or squares. They are used as micro heat spreaders for small thermal hot spots to allow a better heat transfer to a heat sink. They can be machined out of silicon and allow for a thermal conductivity of 8 W/(m K) [50], which is about twice that of copper.

Micro heat pipes are exclusively used for die-sized applications and are not feasible for cooling the antenna array.

6.5.2 Conlusion

Although a heat pipe approach seemed to be promising, it showed that the required power rating for the limited space available cannot be obtained. Referring to Fig. 3.3, the heat pipe width has to be less than 10 mm due to the connector cut outs. The hight is limited to 5 mm due to the assembly constraints. The evaporator length would have to be 12.5 cm (half of the array length), and the total dissipated power for this strip would be 190 W.

To give an example, a high power heat pipe (with sintered copper powder wick structure) from Thermacore can transfer less than 25 W in a circular heat pipe with an outer diameter of 6.25 mm in horizontal orientation [51]. A circular mesh heat pipe from

Quick-Ohm with an outer diameter of 6 mm is capable of transferring about 45 W [52]. An inquiry at Atherm (a French company) confirmed that even a tailored heat pipe heat sink would not fulfill the required power rating.

6.6 Other cooling techniques

Expendable liquid systems. Expendable liquid systems are capable of dissipating large heat loads. As an example it has been reported that the entire 23 kW heat load in an aircraft was dissipated by means of an expendable liquid system [53]. The obvious disadvantages of such a system are that refrigerants have to be refilled regularly. Therefore, they are not being considered for the given problem.

Micro-channel integrated heat sinks. Micro-channel heat sinks are cold plates featuring channels with a width in the micrometer range. Immense heat transfer rates can be obtained; a reported heat flux of 790 W/cm^2 for channel widths of 50 μm has been dissipated for a total square area of 1 cm^2 [54], to give an example. While this technology seems to be promising for modern high speed electronic circuits, where a large amount of heat is dissipated locally, it is not suited for the given cooling problem of a distributed heat source with dimensions around 25×25 cm^2.

Direct immersion cooling. Direct immersion cooling is principally very similar to air cooling. Now, the surrounding fluid, air, has been replaced by a liquid, which is often a dielectric fluid. As for air cooling, several cooling methods can be considered including natural and forced convection. See [55] for an overview. In addition to air cooling systems, two-phase flow can occur and heat transfer can be further increased.

Although this approach would allow to cool both the high frequency amplifiers and all other electronics by one cooling system, the technical challenge of building a sealed system and conditioning the fluid is far superior to a rather simple liquid cooled cold plate. Therefore, this approach is not being considered.

7 Experiments

The background behind conducting experiments was to verify the accuracy of simulation results especially with respect to the liquid cold plate as proposed in Sec. 6.3.2. Furthermore, it was thought to prove the feasibility of the before mentioned design, and to gain practical experience with liquid cold plates in general.

7.1 Design

The performance of the cold plate as described in Sec. 6.3.2 was to be confirmed by experiments. Therefore, a simplified and downsized (less elements) model of the cold plate resembling the general geometry was built. This modified geometry, as shown in Fig. 7.1, was simulated with Flotherm as well to allow a direct comparison of temperature values gained through experiments and simulations.

The built cold plate is shown in Fig. 7.1; detailed dimensions and pictures are given in the Appendix in Fig. A.1 and A.2. The dimensions resemble an array with 12×10 elements. Three liquid channels with a cross-sectional area of 3×1 mm^2 each are positioned between each row of cut outs as well as to their sides (see Fig. A.2(a) for details). The connectors are realized as cut outs in the cold plate. Since tubes had to be connected to the inlet and outlet of the cold plate, the cold plate was extended to support an adapter region. This was thought to provide better stability than two separate adapter regions, which would have to be connected to the middle block, although the dimensions of the extensions are as large as the resembled array itself. The utilized tubes had an inner diameter of 9.5 mm (3/8″), which resulted in a rather large tube fitting. Comparing the cross-sectional areas of the tube (70.9 mm^2) and the total cross-sectional area of all 15 channels (45 mm^2), it becomes apparent that the cold plate acts as a flow resistance. The tube fitting was connected to the cold plate by means of a screw joint, which was detachably sealed by an adhesive.

The actual cold plate (with thickness 4 mm) featuring the milled channels was made out of copper. The cover plate (with thickness 1 mm) was instead made out of brass due to better machining properties of this material. The cover plate and the aluminum screw nut blocks were permanently attached to the copper base plate by means of a thermally conductive adhesive (Elecolit 6601).

Resistors as heat sources. The main heat sources for the antenna array are the amplifiers. They were replaced by (cheap) SMD resistors. The amplifiers have a maximal power dissipation of 3.8 W, and their size is 2.44×1.15 mm^2. There are no SMD resistors commercially available which could cope with such a high power rating featuring such a small footprint. A compromise had to be found, and chip resistors (type PWC) from Welwyn were finally selected [56]. They feature a power rating of 1.5 W at

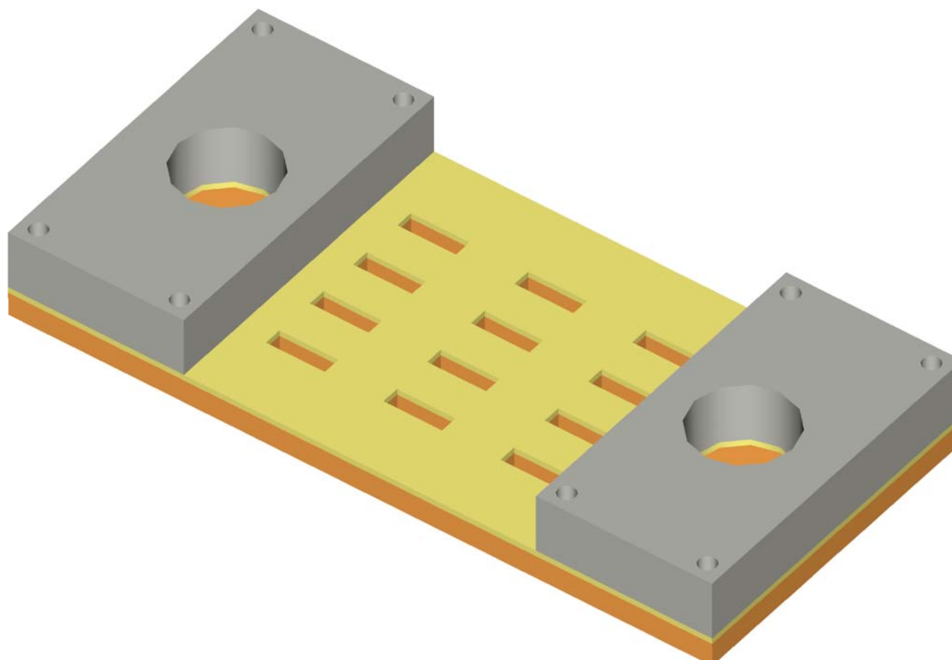

Figure 7.1: Built cold plate; the heat sources are located on the reverse side. It consists of four parts: copper base plate, brass cover plate, and two aluminum blocks featuring screw threads for the tube fittings. Dimensions are shown in Fig. A.1 in the Appendix.

70 °C base plate temperature, occupying a footprint area of 6.5×3.2 mm^2.

One resistor alone already exceeds the area available for one element (of 5×5 mm^2). Since additional space was needed for circuit paths, one resistor finally represented four amplifiers. In total, 30 resistors, with a resistance of 220 Ω (2 %) each, represented therefore 120 amplifiers. One terminal of each resistor was soldered to a printed circuit board (0.2 mm thick, material: FR-4). The other terminal was directly soldered to the copper cold plate, which was utilized as ground. The solder ($\lambda \approx 50$ W/(m K)) was thought to provide good thermal coupling to the cold plate.

The positions of the resistors and the layout of the printed circuit board can be see in Fig. A.3 in the Appendix. The circuit board was bonded to the copper cold plate by means of a thermally conductive adhesive (Elecolit 6601). The same adhesive was used to attach the resistors to the circuit board prior to soldering.

7.2 Thermometer

The used thermometer is the DTM 3080 from LKM electronic [57]. It allows for temperature measurements in the range from $-200 \ldots 820$ °C with an accuracy of 0.1 °C. The utilized temperature sensor is the WTF30 spring loaded tip surface probe from the same company. The approximately circular surface area has a diameter of 2.5 mm. It is a class A Pt100 sensor according to DIN EN 60751, which allows for an accuracy of at least 0.5 K in the interesting temperature range ($0 \ldots 150$ °C). The sensor operating range is $-50 \ldots 400$ °C.

A resistance temperature detector (RTD) based thermometer was chosen as opposed to a thermocouple based one due to the higher accuracy achievable. The accuracy of thermocouples is usually not better than 0.75 % of the temperature for the complete

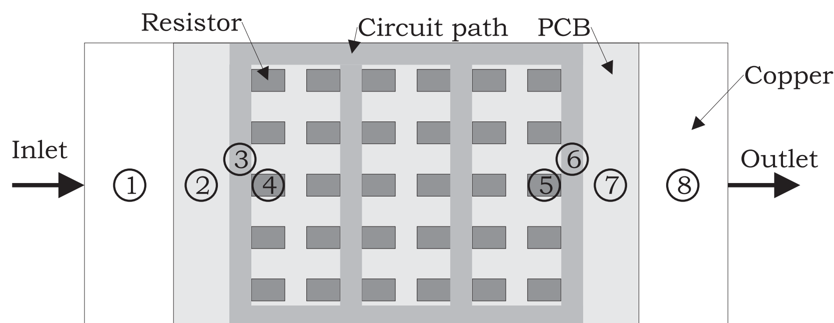

Figure 7.2: Location of measurement points; view from above.

temperature range. RTDs suffer from a slower response time as opposed to thermocouple probes, which is not of major concern for static measurements.

Practical experience. It showed that surface measurements are difficult to perform since the surface probe is not immersed into the object. The flat probe tip had to be very well aligned with the (equally flat) surface under consideration. Very slight changes in alignment resulted in supposedly random temperature steps up to 10 K for measurements at around 70 °C. Reproducible results were not obtainable on uneven surfaces like soldering joints. The use of thermal grease did not improve the predictability of results.

Therefore, a supporting stand for the probe was manufactured in order to enforce a precisely upright orientation of the probe. It was made out of a 50 mm thick plastic block, in which several drilled holes defined the positions of the probe. The so defined positions are indicated in Fig. 7.2. This new approach worked very well for all points except number 4 and 5 (measurement directly at the surface of a resistor). For these two points, by merely turning the probe slightly around its axis, temperature differences of up to 10 K were obtained. This was attributed to two factors: First, the flat area at the probe tip is not exactly orthogonally aligned with respect to the probe axis. This slight misalignment results in a thermal interface which is based on a few contact spots only. The second factor is the high temperature gradient across the resistor surface. By turning the probe, the contact spot was moved along the surface which explains the unreproducible temperature values. Therefore, the temperature values from the spots number 4 and 5 were left out in the discussion of results.

7.3 Experimental setup and execution

Fluid flow. Distilled water was used as the coolant. It was chosen due to its good availability and high specific heat.

The hot spot temperature of the cold plate depends on the liquid flow rate, which had to be measured. Since no flowmeter was available, the volumetric flow rate was gained by measuring the liquid volume which flowed through the cold plate in a certain time. For that, the closed-loop system as shown in Fig. 6.8 was transferred to an open loop system.

A constant flow rate was necessary to perform the temperature measurements for the various measurement spots. The first approach utilized a direct current pump (type

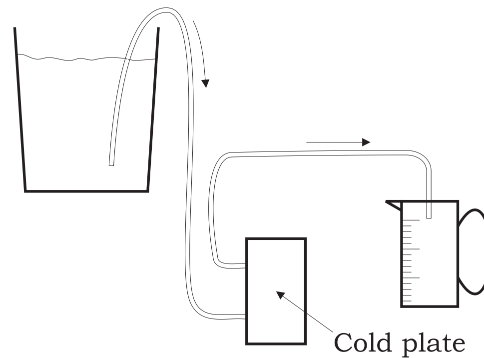

Figure 7.3: Experimental setup without pump. Water flows from a bucket through the cold plate to the measuring cup.

DDC, Laing GmbH), which is usually used as a pump for liquid cooled processors. Although the flow rate can be regulated by varying the pump supply voltage, the minimal flow rate was still above the intended range. Therefore, a flow resistance in form of a fabric at the water inlet was added.

Measurements showed that the flow rate for this setup was not constant over time, it was rather decreasing. This time-variant behaviour was attributed to the pump after it was insured that the introduced inlet flow resistance did not change over time. In order to overcome the problem, the setup according to Fig. 7.3 was built. It is based on the principle of different liquid pressures for different heights in a tube system. The water in the tank (bucket) was manually held at a constant level, and the outlet height was not varied during any one measurement. Differences in height around 20 cm were sufficient to obtain flow rates up to roughly 20 ml/s.

Early measurements confirmed that the flow rate was now constant, but during the course of the experiment it was observed that the flow rate was still decreasing, although slower than for the pump setup. See Sec. 7.7 for a possible but not realized improvement.

Execution. To obtain one set of temperature values (as indicated in Fig. 7.2), the fluid flow rate was set to a specific value by adjusting flow resistances. For each temperature measurement it was assured that the probe tip completely heated up, and the thermometer displayed a constant value. The warmed-up water from the outlet was separated from the inlet water to ensure a constant water inlet temperature for one set of temperature values.

7.4 Simulation

The simulated geometry is shown in Fig 7.4. The adapter regions and the aluminum screw nut blocks are included in the design. Also incorporated are the 0.2 mm thick circuit board and the adhesive layer as well as soldering joints, which thermally connect one resistor terminal to the copper cold plate.

The water flow rate was set to the same values as obtained through measurements. The same was done for the water inlet temperature to allow a direct comparison of simulated and measured values. Pump power was not taken into account since the

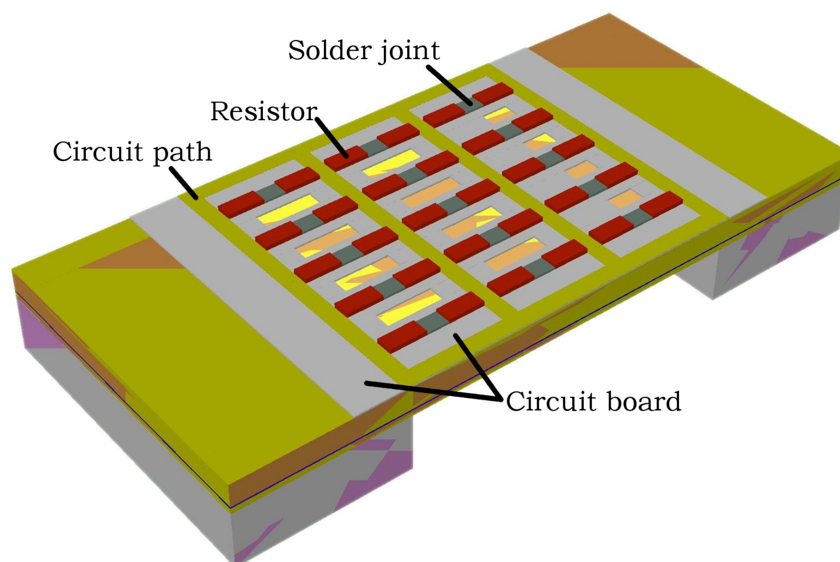

Figure 7.4: Simulated geometry.

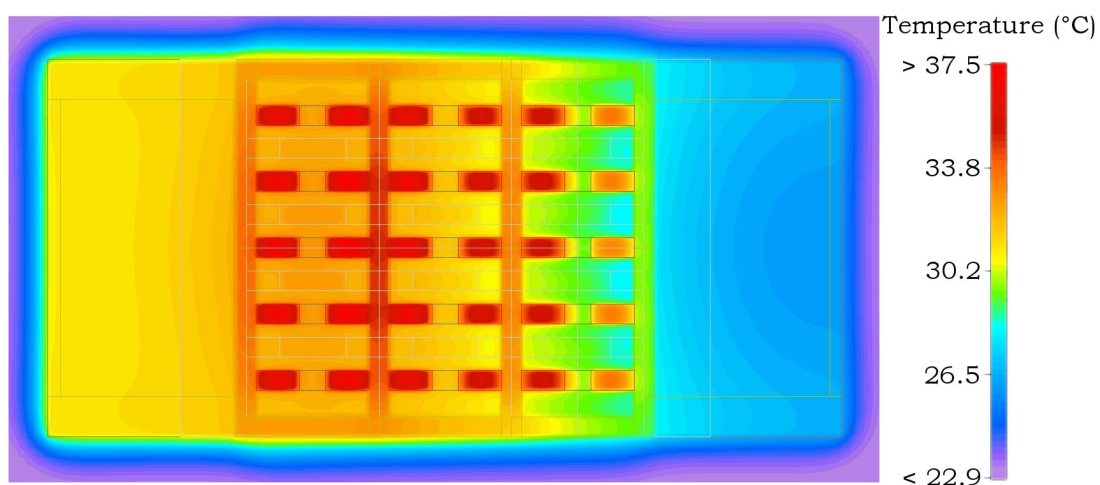

(a) Cut through the layer being directly below the heat sources. The water flows from right to left.

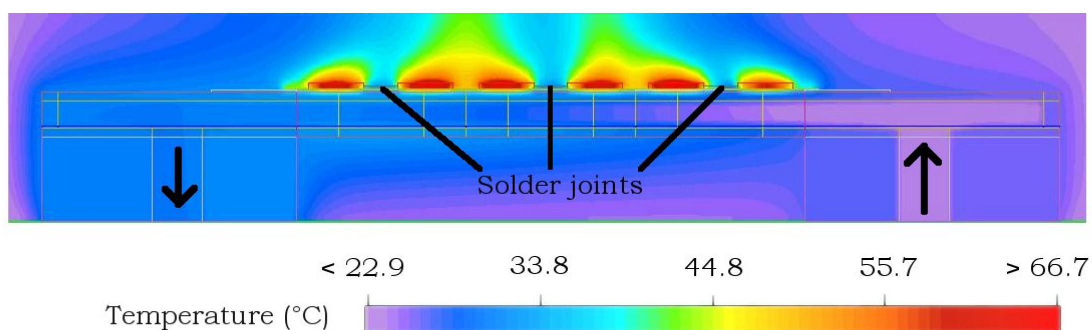

(b) Cut through the middle liquid channel. The effect of the thermally conducting soldering joints can be seen.

Figure 7.5: Computational results for geometry as shown in Fig. 7.4.

measurements were performed without a heat dissipating pump as well.

The temperature distributions for a flow rate of 2.0 ml/s and an ambient temperature (including water temperature at inlet) of 22.9 °Care shown in Fig. 7.5. In Fig. 7.5(a) it can be seen that the circuit paths act like a heat spreader. Figure 7.5(b) shows the insulating effect of the circuit board and the effect of the soldering joints, which guide the heat flux to the cold plate.

7.5 Sources of error

Measured and simulated values do not perfectly coincide. The sources of error for both measurements and simulations will be given.

Measurements. Sources of error for measured data can be attributed to two factors. Measured *temperature values* are imprecise due to the limited accuracy of the probe and meter. According to specifications, the values are precise up to ± 0.35 K at 50 °C. Another source of error is the finite probe size so that the temperature could not be measured at one spot; the measurement values rather represent an average over the probe tip (which results in different values than values obtained through simulations).

The second factor is the time-varying *flow rate*. During the course of obtaining one set of measurements, the flow reduced between 5 % to 30 %. The accuracy of time and volume measurements was superior to this variation and can be neglected.

Simulation. The overall accuracy for Flotherm stated by Flomerics is about ± 2 K. Adding to this basic inaccuracy are errors due to insufficient modelling. Namely, the thermal conductivities of the solder ($\lambda \approx 50$ W/(m K)) and the PCB board ($\lambda \approx 0.3$ W/(m K)) are assumed values, and variations for these values effect the overall temperature distribution.

The simulated model was simplified in so far as the tube fitting was left out, and a square cross-sectional area was implemented instead of a circular one. This is due to the limitations imposed by the Cartesian system grid. The overall error introduced by these simplifications is assessed to be small.

The fluid flow at the outlet adapter region could not be sufficiently modeled. This is due to turbulence which was encountered at the channel outlets, and which could not be described in a steady state solution. Flotherm's output suggested nevertheless that the temperature values should be accurate.

Another distinction between simulation and experiment was the orientation of the cold plate with respect to gravity (which is the cause for heat transfer by natural convection). On the other hand, simulations showed that temperatures were practically identical for different orientations.

Design. It could not be verified if the volumetric fluid flow rate was equal for all channels. A possible design improvement is given in Sec. 7.7.

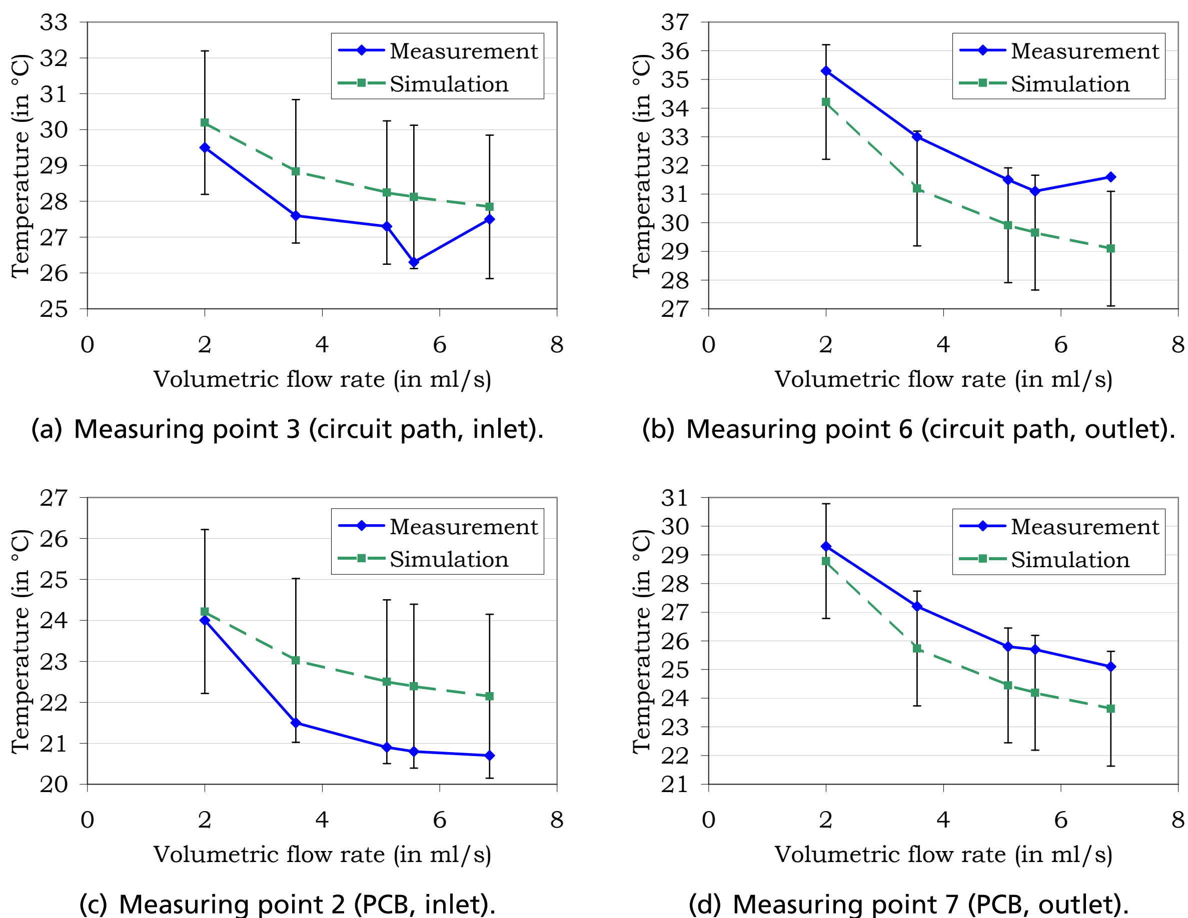

(a) Measuring point 3 (circuit path, inlet).

(b) Measuring point 6 (circuit path, outlet).

(c) Measuring point 2 (PCB, inlet).

(d) Measuring point 7 (PCB, outlet).

Figure 7.6: Comparison of experimental and simulation results; numbering according to Fig. 7.2. Error bars represent Flotherm's accuracy of ± 2 K.

7.6 Results and discussion

Since the water inlet temperature was not the same for all measurements, all values were shifted to reflect a constant water inlet temperature of 20 °C. This allows for direct comparison of all temperature values.

The comparison between measurement and simulation are shown in Fig. 7.6 for measuring points 2, 3, 6, and 7. The values for measuring points 4 and 5 (directly on the resistors) were discarded due to effects described in Sec. 7.2. The graphs include error bars (± 2 K), which indicate the accuracy of Flotherm. It can be seen that except for one value in Fig. 7.6(b) all measured temperature values lie within this accuracy. If one would indicate the error bars for the measurement values as well (at least ± 0.35 K due to the thermometer accuracy neglecting other effects), it becomes apparent that coherent results were obtained for all values.

The shape of the curves complies with theory. For flow rates from 2 ml/s to 6.85 ml/s, the Reynolds number ranges from 74 to 255, assuming the same volumetric flow rates through each channel. This indicates laminar flow. For laminar flow, the heat transfer does not depend on the flow rate, which would influence ΔT_B in Eq. (6.4). On the other hand, ΔT_A according to the same equation is inversely proportional to the mass flow rate, explaining the hyperbolic shape.

It can be concluded that the accuracy of Flotherm for this computational model is at least ± 2 K. This supports the choice of Flotherm as the computational tool. Since the

geometry resembles quite closely the one of the proposed cold plate for an array with 50 × 50 elements (see Sec. 6.3.2), it can be justifiably assumed that these simulation results are accurate up to ±2 K as well.

Practical experience. The practical experience with the liquid cold plate was positive throughout the project. It could be manufactured without special tools in a reasonable time. No liquid leakage occurred whatsoever. The cold plate made a very robust impression which allows the cold plate to be used as a mechanical support for the antenna array as well.

7.7 Improvements

Although the definite cause for the decreasing liquid flow rate could not be found, it seems to be possible that the (slow) liquid flow was obstructed by accumulated air in the system and especially by air bubbles in the small liquid channels. This could explain the gradual decrease of the flow rate and the increase after the system had been at rest for a while.

To prove this point, a transparent cover plate (e. g. glass, acrylic glass) could replace the brass plate to allow observation of the liquid flow. By this approach and using colored water, it could be as well examined if the fluid velocity in the channels is uniform for all channels (as is suggested by simulations). Since the brass plate was permanently attached (by means of adhesive) to the cold plate, this approach could not be followed during the course of this project.

8 Heat exchanger

At this stage of the ATENAA project investigations have been directed towards showing that an Ka band antenna array could generally be build. Detailed analysis of a later installation was excluded so far, and that is why the development of the cooling system concentrated simply on heat extraction rather than the development of a complete cooling loop as shown in Fig 6.8. Nevertheless, the heat exchanger is an important part of a closed loop liquid cooling system as proposed in Sec. 6.3 so that general ideas will be presented here.

The heat exchanger has to ensure that the warm water is sufficiently cooled down before it enters the cold plate again. A typical approach of dissipating heat in aviation electronics is by means of air cooling. Cool air is supplied by the aircraft's environmental control system (ECS). The worst-case total dissipated power of all power amplifiers (not including other electronics) for a 50×50 element array is 9.5 kW, which adds considerable to the heat load for the ECS. If an air-cooled heat exchanger is used, it has to be ensured that the ECS can cope with the added head load.

To give an idea of the required heat exchanger size, a commercially available air cooled heat exchanger was selected as an example. The selection was based on the following assumptions:

- maximum heat load of 9.5 kW,
- air inlet temperature of 20 °C,
- fluid is water,
- water inlet temperature of 55 °C, and
- water flow rate of 0.125 l/s.

A heat exchanger from Lytron, type 6340, meets the requirements [43]. The thermal resistance is 280.5 W/K at a liquid flow rate of 0.125 l/s. The outer dimensions (excluding fans) are $630 \times 564 \times 89$ mm^3. The recommended fan type (four fans are needed for this heat exchanger) is from Comair Rotron, type Caravel, which adds another 89 mm (totalling to 178 mm) to the overall height of the complete heat sink. This simple example shows that heat exchanger dimensions are still reasonable considering the cabinet size constraint of $2 \times 1 \times 0.3$ m^2 as defined by the ATENAA project. Nevertheless, the heat exchanger takes up valuable space.

An advantage of a liquid cooled system is that heat (i. e. the warm liquid) can easily be transfered over a longer distance. It would be possible to exclude the heat sink from the cabinet in which the complete antenna module is mounted.

Another approach to heat rejection than air cooling is to transfer heat to the aircraft fuel [34]. This cooling method and its correlated problems are very specific to the actual aicraft and beyond the scope of this work.

In order to lower the heat load on the environmental control system, a heat sink based on expendable coolants could be used [34]. The principle is that a high amount of heat can be dissipated due to the latent heat of a coolant. The evaporated medium is then disposed to the outside of the aircraft. The disadvantages are that additional mass has to be transported, and that the cooling system has to be regularly refilled. Therefore, this scheme is not likely to be incorporated into commercial aircrafts.

9 Conclusion

The question under consideration was if a cooling system for an active antenna array in the Ka band could be developed. Several cooling technologies including forced air and liquid cooling as well as heat pipe cold plates were examined.

Forced air cooling systems are not able to cope with the high heat load of a full-sized antenna array given the assembly constraints. Nevertheless, a forced convection fin heat sink based on standard components was proposed for an array of 4×4 elements (see Sec. 6.2.2). This can be used as a cooling system for an antenna demonstration model.

Although heat pipes are a promising approach for many applications due to their high heat transfer capabilities and a passive, sealed system, the required heat loads could not be transfered (see Sec. 6.5). This resulted from assembly constraints which limited the highest possible cross-sectional area of the heat pipes.

Simulations using Flotherm showed that a liquid cold plate is very well suited to fulfill all requirements (see Sec. 6.3). A worst case heat load of 9.5 kW for an array of 50×50 elements can be dissipated. Experiments on a simplified (i. e. smaller) model confirmed the practical feasibility of the cold plate (see Ch. 7). Comparison of measurements and simulations showed good agreement between both, which reinforced the decision to use the stated software.

A Detailed drawings and pictures of cold plate

On the following pages, detailed drawings and pictures of the built cold plate are shown.

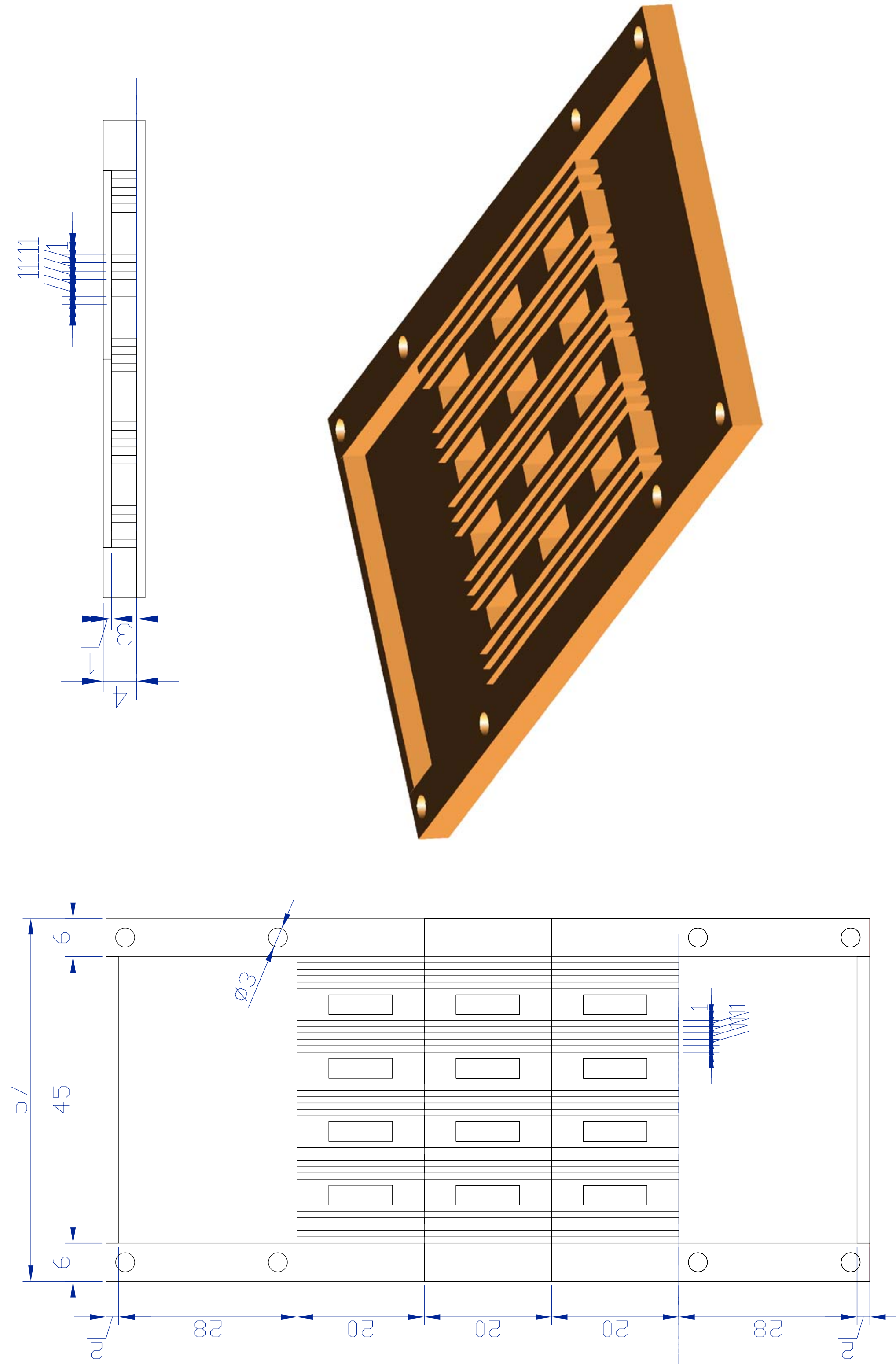

(a) Copper cold plate with fluid channels.

Figure A.1: Built liquid cold plate. All dimensions in mm.

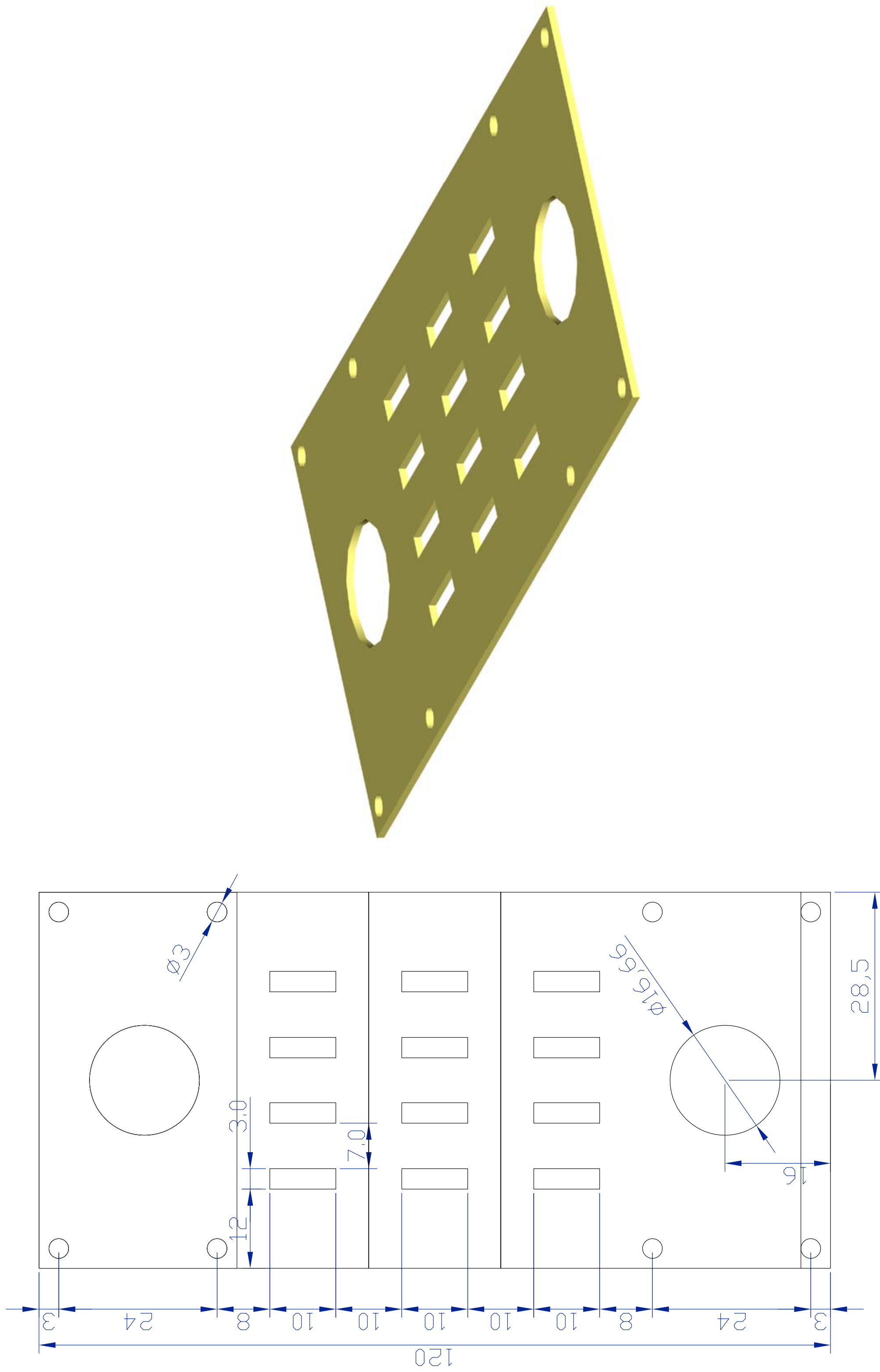

(b) Brass cover plate.

Figure A.1: Built liquid cold plate.

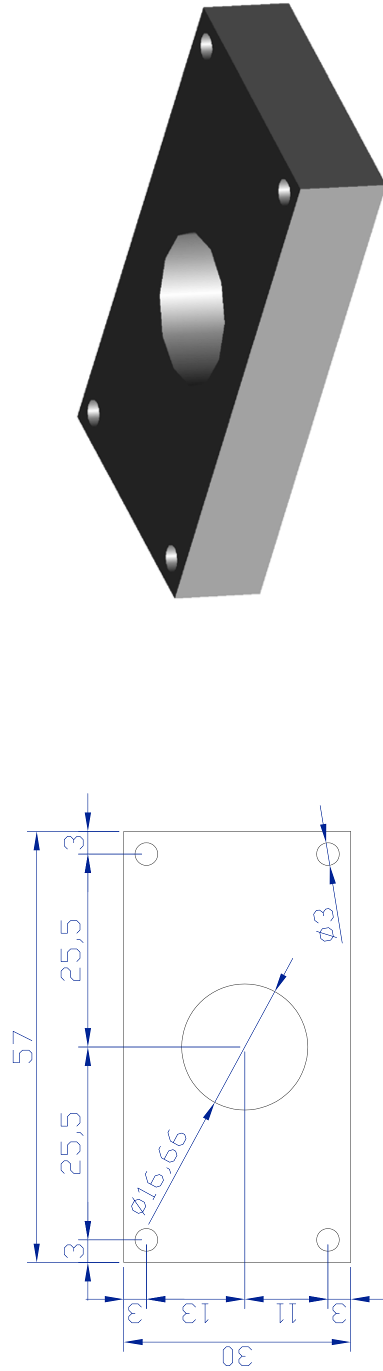

(c) Aluminum screw nut.

Figure A.1: Built liquid cold plate.

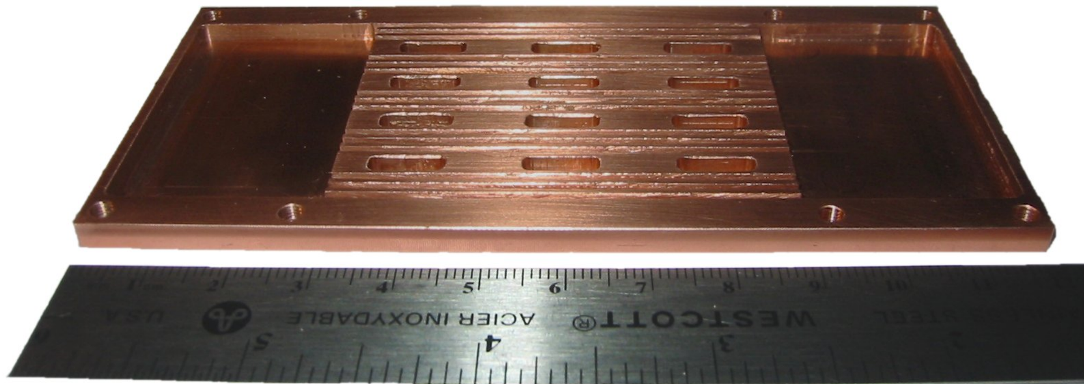

(a) Copper base plate featuring channels.

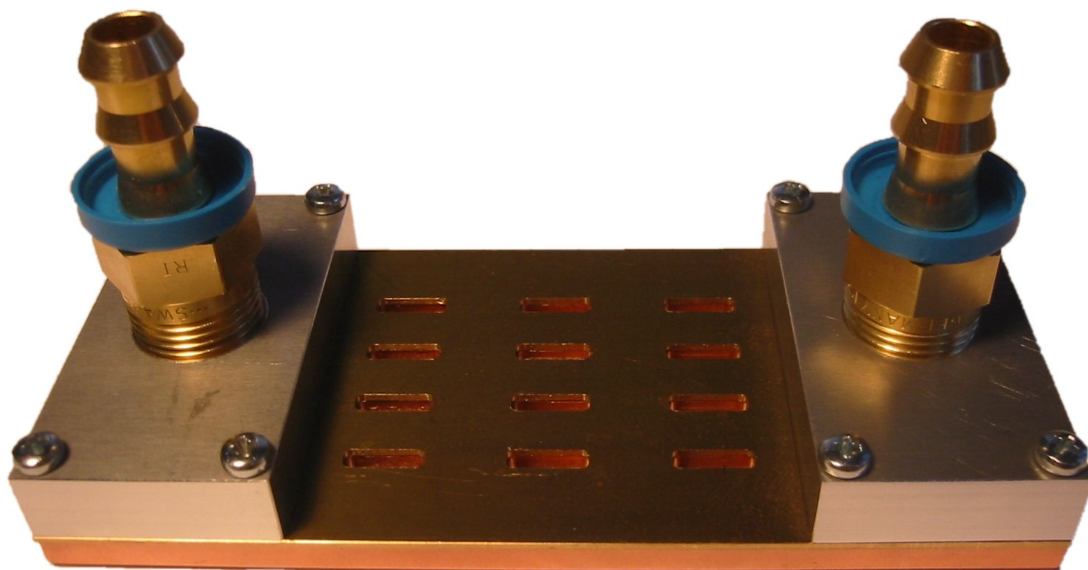

(b) Complete cold plate including inlet and outlet. The heat sources (resistors) are located on the reverse side.

Figure A.2: Picture of the build cold plate. The cut outs resemble the positions of the connectors.

Figure A.3: Circuit board for built liquid cold plate. The 0.2 mm thick substrate was milled to allow one terminal of each resistor to be soldered directly to the copper base plate.

Bibliography

[1] Christian Hunscher, Michael Thiel, Achim Dreher, Sybille Holzwarth, Leif C. Stange, Holger Pawlak, Alexander Molke, and Arne F. Jacob. SANTANA – Smart antenna terminal, final report. Technical report, EADS Astrium, DLR, IMST GmbH, and TU Braunschweig, 2004.

[2] RTCA, Inc., Washington, DC. *RTCA/DO-160D. Environmental Conditions and Test Procedures for Airborne Equipment*, July 1997.

[3] Normenstelle Luftfahrt im DIN Deutsches Insitut für Normung e. V. *DIN ISO 2533: Normatmosphäre*, December 1979.

[4] H. Zeffert. *Principles and Practice of Aircraft Electrical Engineering*. George Newnes Limited, London, 1960.

[5] Maximilian Wutz. *Wärmeabfuhr in der Elektronik*. Vieweg, 1991.

[6] Joe Yoon. Concorde history II. Retrieved September 29, 2005 from the World Wide Web: `http://www.aerospaceweb.org/question/planes/q0199.shtml`, 2004.

[7] TriQuint Semiconductor 27–31 GHz 1 W power amplifier TGA4509-EPU data sheet, January 2005.

[8] Iridium Corporation of America. *Eutectic Gold/Tin Solder. Product Data Sheet*, 2005.

[9] Dwight E. Gray, editor. *American Institute of Physics Handbook*. McGraw-Hill, second edition, 1963.

[10] S. I. Novikova. Investigation of thermal expansion of GaAs and ZnSe. In John S. Blakemore, editor, *Gallium Arsenide*. American Insitute of Physics, Original article submitted June 13, 1960. Reprinted from Soviet Physics – Solid State, vol. 3, (1961).

[11] Mark Occhionero, Richard Adams, and Kevin Fennessy. A new substrate for electronic packaging: Aluminum-silicon carbide (AlSiC) composites. In *Proceedings of the Forth Annual Portable by Design Conference, Electronics Design*, pages 398–403, March 1997.

[12] David L. Saums. Developments in selective high thermal conductivity orientation in CTE-compatible substrate and package component materials. In *Semiconductor Thermal Measurement and Management Symposium*, March 2004.

[13] Jeanne Pavio and Don Hyde. Effects of coefficient of thermal expansion mismatch on solder attached GaAs MMICs. In *IEEE Microwave Symposium Digest*, volume 3, June 1991.

[14] Tom Tuhus and Are Bjorneklett. Thermal cycling reliability of die bonding adhesives. In *International Reliability Physics Symposium*, March 1993.

[15] Horst Stöcker, editor. *Taschenbuch der Physik*. Verlag Harri Deutsch, Thun and Frankfurt am Main, third edition, 1998.

[16] Wolfgang Beitz and Karl-Heinz Küttner, editors. *Taschenbuch fü den Maschinenbau / Dubbel*. Springer, 17th edition, 1990.

[17] Massachuchetts Institute of Technology OpenCourseWare. Retrieved from the World Wide Web November 2, 2005: `http://ocw.mit.edu/NR/rdonlyres/Materials-Science-and-Engineering/3-11Mechanics-of-MaterialsFall1999/698ECA59-8F00-46CC-96A1-B9365CBD63E3/0/props.pdf`, 1999.

[18] Collaboration. Authors and Editors of the LB Volumes III/17A-22A-41A1b. *Gallium arsenide (GaAs), Debye temperature, density, heat capacity, melting point*, volume 41. Subvolume A1A/2001 of *Landolt-Börnstein - Group III Condensed Matter*. Springer-Verlag GmbH, January 2001.

[19] *GaAs MMIC ESD, Die Attach and Bonding Guidelines*, May 2000. Agilent Technologies, Application Note no. 54 – Rev. A.

[20] Klaus Langenheinecke, editor. *Thermodynamik für Ingenieure*. Viewegs Fachbücher der Technik, 1993.

[21] Ulrich Grigull and Heinrich Sandner. *Wärmeleitung*. Springer-Verlag, Berlin, 1979.

[22] Klaus Gersten. *Einführung in die Strömungsmechanik*. Verlag Vieweg, sixth edition, 1991.

[23] Walter Wagner. *Wärmeübertragung*. Kamprath-Reihe. Vogel Buchverlag, third edition, 1991.

[24] Erich Truckenbrodt. *Lehrbuch der angewandten Fluidmechanik*. Springer-Verlag, 1983.

[25] U. Grigull, H. Sandner, J. Straub, and H. Winkler. Origins of dimensionless groups of heat and mass transfer. Retrieved from the World Wide Web on December 9, 2005: `http://www.ichmt.org/dimensionless/dimensionless.html`, 1982. On the occasion of the 7th interational Heat Transfer Conference, München.

[26] Dave S. Steinberg. *Cooling Techniques for Electronic Equipment*. A Wiley-Interscience Publication. John Wiley & Sons, 1980.

[27] McCarthy. Convective heat transfer example. Retrieved from the World Wide Web December 9, 2005: `http://granular.che.pitt.edu/~mccarthy/che1011/Intro/Conv/conv_a.html`.

[28] Hans Dieter Baehr and Karl Stephan. *Wärme- und Stoffübertragung*. Springer-Verlag, 1994.

[29] *User's Manual. Thermal Desktop – A CAD based system for Thermal analysis and Design. Version 4.7, Patch 3.*, October 2004.

[30] David A. Johnson, Mark J. Welch, and Brent A. Cullimore. Novel simulation techniques for design of air-cooled electronics. In *Proceedings of InterPack '01*, July 2001.

[31] Flomerics Limited, Surrey, England. *Getting Started with FLOTHERM – For software version 5.1*.

[32] Robin Bornoff. Validation of localized grid in version 4.2. Technical report, Flomerics Ltd., November 2003.

[33] Christopher Hess. Technology for the good climate on board. *Flug Review*, October 1999.

[34] P. W. Smith, editor. *Avionic Cooling and Power Supplies for Advanced Aircraft*. North Altantic Treaty Organization. Advisory Group for Aerospace Research and Development, June 1976.

[35] Maik Turner. All you need to know about fans. *Electronics Cooling*, 2(2), May 1996.

[36] C. L. Belady. Design considerations for air cooling electronic systems in high altitude conditions. *IEEE Transactions on Components, Packaging, and Manufacturing Technology*, 19(4), 1996.

[37] James Edwin Marthinuss Jr. and George Thomas Hall. Cooling electronics at high altitudes made easy. *Electronics Cooling*, 4(3), 1998.

[38] PTI Pelonis Technologies, Inc. *DC Blower 1230*, 2005.

[39] CofanUSA, Fremont, CA. *DC Brushless Fan Motor – 50 * 50 * 20 mm*. Retrieved from the WWW on November 20, 2005: `http://www.cofan-usa.com/New/fans/dc_fans/50x20/50x20.PDF`.

[40] Panacol-Elosol GmbH. *Elecolit® 6601*. Technisches Datenblatt.

[41] L. S. Fletcher. A review of thermal enhancement techniques for electronic systems. In *InterSociety Conference on Thermal Phenomena in Electronic Systems*, May 1990.

[42] Rf dummy loads, calorimeters and cooling equipment for electronics, catalog 2000.

[43] Lytron. *Lytron – Total Thermal Solutions, 2004 Catalog*, 2004.

[44] C. K. Loh, Enisa Harris, and D. J. Chou. Comparative study of heat pipes performances in different orientations. In *Semiconductor Thermal Measurement and Management Symposium*, pages 191–195. IEEE, March 2005.

[45] Adrian Bejan and Allan D. Kraus. *Heat Transfer Handbook*. John Wiley & Sons, Inc., 2003.

[46] Mohamed Chaker Zaghdoudi, Christian Tantolin, and Claude Godet. Flat heat pipes thermal performance in body force environment. In *Inter Society Conference on Thermal Phenomena*, 2000.

[47] Shankara Narayanan K.R. What is a heat pipe. Retrieved from the World Wide Web November 28, 2005: `http://www.cheresources.com/htpipes.shtml`.

[48] Beate Unger. 10 wichtige regeln für die verwendung von heatpipes. Retrieved from the World Wide Web November 30, 2005: http://www.quick-cool-waermetransfer.de/heatpipe/download/10-Regeln_Heatpipe.pdf.

[49] C. B. Sobhan. Miniaturization: Modern trends in heat pipe technology. Retrieved from the World Wide Web November 26, 2005: file:///H:/docs/cooling-techniques/heat-pipes/Miniaturization%20Modern%20Trends%20in%20Heat%20Pipe%20Technology.htm.

[50] D. A. Benson, R. T. Mitchell, M. R. Tuck, D. R. Adkins, and D. W. Palmer. Micromachined heat pipes in silicon mcm substrates. In *Multi-Chip Module Conference*. IEEE, February 1996.

[51] Thermacore International, Inc. *HP-1 Heat Pipe*, 2000.

[52] Standard-heatpipe mesh rund. Retrieved from the World Wide Web December 10, 2005: http://www.quick-cool-waermetransfer.de/heatpipe/heatpipe-mesh/heatpipe-mesh.html.

[53] Donald C. Price. A review of selected thermal management solutions for military electronic systems. In *IEEE Transactions on Components and Packaging Technologies*, volume 26, March 2003.

[54] D. B. Tuckerman and R. F. W. Pease. High-performance heat sinking for VLSI. In *IEEE Electron Device Letters*, volume EDL-2, May 1981.

[55] Issam Mudawar. Direct-immersion cooling for high power electronic chips. In *InterSociety Conference on Thermal Phenomena*. IEEE, 1992.

[56] TT electronics – Welwyn Components, UK. *Pulse Withstanding Chip Resistors*, October 2005.

[57] LKM electronic GmbH. *DTM3000 für Pt100/Pt1000*, June 2005. Identical in construction to DTM3080.